Preprints (www.preprints.org) | NOT PEER-REVIEWED | Posted: 11 October 2019 doi:10.20944/preprints201910.0123.v1

Peer-reviewed version available at *Remote Sens.* **2019**, *11*, 2652; doi:10.3390/rs11222652

Assessment of Integrated Water Vapor Estimates from the iGMAS and the Brazilian Network GNSS Ground-Based Receivers in Rio de Janeiro

Galdino Viana Mota [1,2,*], Shuli Song [2,*], and Katarzyna Stępniak [3]

[1] Shanghai Astronomical Observatory (SHAO), Chinese Academy of Sciences (CAS), China; slsong@shao.ac.cn
[2] Universidade Federal do Pará, Belém, Brazil; galdinov@ufpa.br
[3] University of Warmia and Mazury in Olsztyn, Poland; katarzyna.stepniak@uwm.edu.pl
* Correspondence: slsong@shao.ac.cn; galdinov@ufpa.br; Tel.: +86-021-3477-5240 (S.S.)

Abstract: There is crescent demand for knowledge improvement of the integrated water vapor (IWV) distribution in regions affected by heat islands that are associated with extreme rainfall events such as in the metropolitan area of Rio de Janeiro (MARJ). This work assessed the suitability and distribution of IWV in the MARJ using products from the Global Navigation Satellite Systems (GNSS), MODerate Resolution Imaging Spectroradiometer (MODIS), and radiosonde. GNSS data were collected by the tracking station named RDJN, from the cooperation of the International GNSS Monitoring and Assessment System (iGMAS) and the National Observatory of Brazil (*Observatório Nacional* - ON), and the tracking stations ONRJ, RIOD, and RJCG belonging to the Brazilian Network for Continuous Monitoring (RBMC) in the period of January 2015–August 2018. High variability of the near surface air temperature (*T*) and relative humidity (*RH*) were observed among eight meteorological sites considered. The mean *T* differences between sites, up to 4.4 °C, led to mean differences as high as 3.1 K for weighted mean temperature (T_m) and hence 0.83 mm for IWV differences. The performance of the MODIS MOD07 and MYD07 products provided a reasonably good representation of the mean spatial distribution of IWV, especially during the daylight passages of the satellites TERRA and AQUA. Local grid points of MODIS IWV estimates had relatively good agreement with the GNSS-derived IWV, with mean differences from -2.4–1.1 mm considering only daytime passages of the satellites TERRA and AQUA. During nighttime, MODIS underestimated IWV (from -9–-3 mm) with respect to GNSS, due to attenuation of IR radiation by clouds. A contrasting behavior was found in the radiosonde IWV estimates compared with the estimates from GNSS. There were dry biases of 1.4 mm (3.7% lower than expected) by radiosonde IWV during the daytime considering that all other estimates were unbiased and the differences between IWV_{GNSS} and IWV_{RADS} were consistent. Based on the IWV comparisons between radiosonde and GNSS at nighttime, the atmosphere over the radiosonde site is about 1.2 (2.3) mm wetter than over RIOD (RDJN) station. The long time series of the comparisons between IWV_{RDJN} and IWV_{RIOD} showed that the highest values of IWV occurred from the afternoon to nocturnal hours. Further, the atmosphere over the site RIOD was consistently about 1 mm wetter than over RDJN. These results showed the feasibility of the iGMAS RDJN station data compared with the RBMC, MODIS, and radiosonde data to investigate IWV in a region with occurrence of heat islands, and the peculiar physiographic and meteorological characteristics as in the MARJ. This work recommended the usage of complete meteorological station data collocated near every GNSS receiver aiming improvements of local GNSS IWV estimates and serving as additional support for operational numerical assimilation, weather forecast, and nowcast of extreme rainfall events.

Keywords: IWV, GNSS, iGMAS, RBMC, meteorological data, MODIS, radiosonde, Rio de Janeiro.

1. Introduction

The development of satellite navigation system has become an essential infrastructure for many countries not solely for military proposes. The advances in this area pursue extensive documentation since the establishment of the Global Navigation Satellite Systems (GNSS) in the last decade of the 20th century. Studies in the recent decades demonstrate the importance of remote sensing applications of GNSS in the fields of navigation, positioning, timing, communication, telemetry, meteorology, and so on. Although the main contemporary systems (US Global Positioning System (GPS), Russian Global Navigation Satellite System (GLONASS), Chinese BeiDou Navigation Satellite System (BDS), and EU Galileo) are well-advanced, there is always demand for precision and accuracy in all fields and applications of GNSS.

GNSS meteorology has gained special relevance for its accuracy and high temporal resolution of all-weather integrated water vapor (IWV) with relatively low costs [1-8]. It is an arduous task to perform accurate measurements with high spatial and temporal resolution of water vapor in the troposphere, which is important for monitoring the evolution of deep convection and precipitation [9-12]. GNSS meteorology constitutes an additional source of IWV estimation, which is also useful in data assimilation in numerical models for weather forecasting and climate studies. Its usefulness is notable in investigations of the space-temporal distribution of water vapor in regions with peculiar physiographical and meteorological characteristics [12] that are not well-represented e.g. by a few daily operational water vapor estimates from radiosonde.

Field experiments and observations over long periods using GNSS meteorology have been conducted in some places in the Subtropics and in the Tropics [9-11,13-15]. The potential benefits of the GNSS applications of Meteorology in Brazil, especially in the Numerical Weather Prediction (NWP), are increasing in the last decades [16-18]. Due to the high quality of the temporal estimation of GNSS IWV compared with radiosonde estimates, GNSS IWV has been considered feasible for climate investigations and for operational numerical assimilation [15,17,19-22].

The installation in 2014 of the ground based GNSS and meteorological stations, named RDJN and RD, respectively, provided an additional source of raw observation and monitoring data useful for all applications. These stations were result of an objective of the International GNSS Monitoring and Assessment System (iGMAS) project in promoting international GNSS monitoring. It was part of an agreement between the Shanghai Astronomical Observatory (SHAO) of the Chinese Academy of Sciences (CAS) and the National Observatory of Brazil (*Observatório Nacional* – ON, Rio de Janeiro).

Rio de Janeiro, the capital of the State with the same name, is located in the southeast region of Brazil. The metropolitan area of Rio de Janeiro (MARJ) is marked by unique physiographic characteristics with complex topography. Its northern border is limited by the city of *Xerém* on the foothills of a large mountain range; while the city of Rio de Janeiro has its southern (eastern) border with the Atlantic Ocean (Guanabara Bay). There are three massive mountain ranges in the city of Rio de Janeiro, covered with vegetation and surrounded by high populated urban and suburban areas. The authors of [23-25] mapped heat islands in the urban, suburban, and rural sectors of the MARJ. Those phenomena have been associated with high records of surface temperature and near surface air temperature (T) that favor the occurrences of extreme rainfall and flooding events that affect the MARJ [26-28]. However, further refinements and validations need to be made to better understand water vapor distributions in regions with complex topography and physiography such as those observed in that region.

This work evaluated the variability of meteorological parameters in the MARJ and in the city of *Campos dos Goytacazes* (located in a flat region in the NE of the State of Rio de Janeiro) and its influences in the calculation of the IWV GNSS. Further, it assessed the suitability of the data from iGMAS RDJN tracking station to estimate water vapor. Moreover, it compared long time series of RDJN IWV estimates with those provided by three receivers from the Brazilian Network for Continuous Monitoring (RBMC, described in detail by [29-32]). GNSS IWV data from the MODerate-Resolution Imaging Spectroradiometer (MODIS) products were also used to evaluate the space distribution of water vapor in two specific regions in the State of Rio de Janeiro and from radiosonde soundings in the city of Rio de Janeiro.

2. Materials and Methods

2.1. Sites and Meteorology Data

 doi:10.20944/preprints201910.0123.v1

Peer-reviewed version available at *Remote Sens.* **2019**, *11*, 2652; doi:10.3390/rs11222652

The GNSS ground-based stations used in this work, named RDJN, ONRJ, and RIOD, were located in the city of Rio de Janeiro, and RJCG located in *Campos dos Goytacazes* (about 230 km ENE from the city of Rio de Janeiro) (see Figure 1 and Table 1).

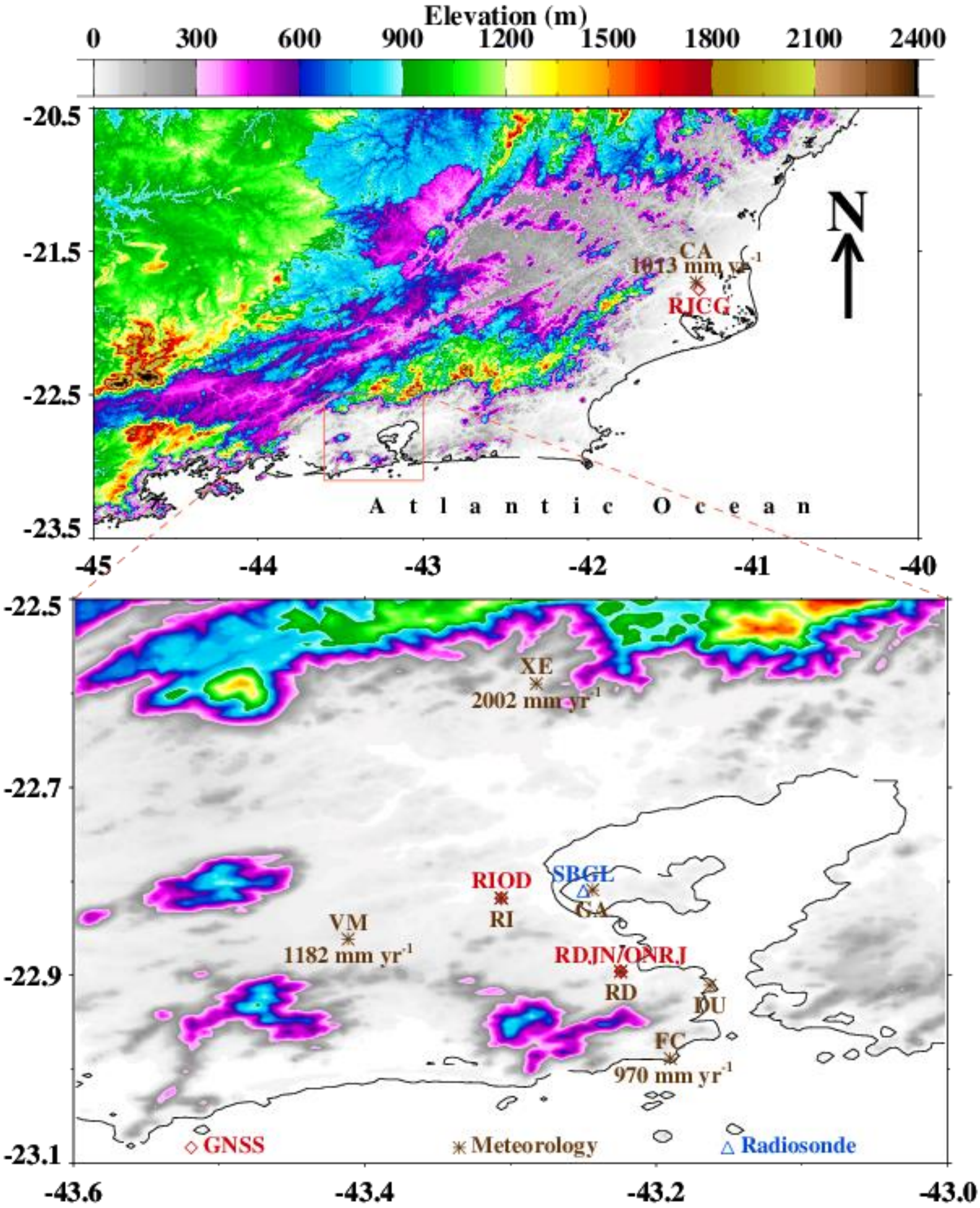

Figure 1. Topography (m) of the State of Rio de Janeiro (upper panel) and the zoomed metropolitan area of Rio de Janeiro (MARJ, lower panel); with the locations of the Global Navigation Satellite Systems (GNSS), radiosonde, and meteorological stations; and the yearly rainfall averages (mm yr^{-1}) from the Instituto Nacional de Meteorologia (INMET) [33] stations for the period of January 2015–August 2018. (See [34] for the source of the elevation data.)

Table 1. Altitude of the GNSS sites, and Receiver and Antenna types used.

Site (Program)	Altitude (m)	Receiver Model	Antenna Model	Installation date
RDJN (iGMAS)	39.45	- UNICORE UB4B0I	- NOV750.R4 NOVS	20 August, 2014
ONRJ (RBMC)	39.53	- LEICA GR25 - TRIMBLE NETR8	- LEICA AR10 (773758) - GNSS CHOKE RING (TRM59800.00)	04 July, 2013 11 March, 2015
RIOD (RBMC)	12.44	- LEICA GR25 - TRIMBLE NETR9	- LEICA AR10 (773758) - ZEPHYR 3 GEODETIC (TRM115000.00)	08 August, 2013 12 March, 2018
RJCG (RBMC)	14.74	- TRIMBLE NETR5	- ZEPHYR GNSS GEODETIC MODEL 2 (TRM55971.00)	11 December, 2007

The iGMAS station RDJN was installed 4 m away from the RBMC station ONRJ in a steel pier base of 3 m height above the concrete roof of a building in the National Observatory. The National Observatory is located on a hill distant about 4 km north and east of a large massive mountain, and 1 km west of the Guanabara Bay. The RBMC station RIOD was installed in a concrete pillar of about 1 m height above the roof in a building of the *Instituto Brasileiro de Geografia e Estatística* (IBGE), located in a valley 12 km NW of the RDJN station and 6 km WSW of the Radiosonde station named RADS located in the Governor's Island (*Ilha do Governador*) in the Guanabara Bay. The RBMC station RJCG was installed in a concrete pillar of 1.2 m height above the roof a building in the *Universidade Federal Fluminense* in *Campos dos Goytacazes*. The city of *Campos dos Goytacazes* is located in a flat region, but distant 28 km east of mountain ranges; and it is distant 31 and 43 km west and north, respectively, of the Atlantic Ocean.

The meteorological data used, as indicated in Figure 1, are from three different sources: (i) the stations near the GNSS receivers—RD alongside the iGMAS station RDJN, and RI alongside the RBMC station named RIOD [29]—; (ii) data from the INMET [33]—the stations VM, FC, XE, and CA—; and (iii) the stations GA[1], , and DU from the Integrated Surface Database (ISD) [35,36]. The meteorological data were available in the period of January 2015–August 2018, except those from RI, which were interrupted by late 2015.

The meteorological data from different inputs for the year 2015 were used to test the values of the observed T and their resulting calculated surface temperature (T_s) and the weighted mean temperature (T_m), and the observed and calculated surface pressure (P and P_s). The best match of meteorological values with those from RI in 2015 were chosen to calculate IWV for the station RIOD in the whole period from 2015–2018.

The data from the station RD (RI) had original time resolution of 1 second (minute), while the others were recorded hourly. The meteorological records were averaged or interpolated for every 15 minutes to match with the time resolution of the total zenith delay (ZTD) outputs to calculate IWV.

2.2. GNSS ZTD and IWV

ZTD is defined as the propriety of the atmosphere to delay electromagnetic waves from the satellites to the receivers in the zenith direction. GNSS signals delayed in the zenith direction are divided, as showed by [1,37,38], into zenith hydrostatic delay (ZHD, with the largest contribution of the dry air atmospheric gases) and zenith wet delay (ZWD, which is produced solely by the atmospheric water vapor):

---

[1] The meteorological station GA, with an elevation of 8.5 m, is located in the International Airport of *Galeão*, near the radiosonde launching site.

$$\mathrm{ZTD} = \mathrm{ZHD} + \mathrm{ZWD}, \tag{1}$$

where

$$\mathrm{ZHD} = 10^{-6} \mathrm{k_1 R_d} \frac{\mathrm{P_s}}{\mathrm{g_m}}, \tag{2}$$

where

$$g_m = \frac{\int_0^\infty \rho_v(z) g(z) dz}{\int_0^\infty \rho_v(z) dz}. \tag{3}$$

The IWV content is referred also as the precipitable water vapor, which is equivalent to the height (in mm) of liquid water obtained if the total mass of water vapor contained in an atmospheric air column of unit cross-section area that were condensed and brought to the receiver's level:

$$\mathrm{IWV} = \int_0^\infty \rho_v(z) dz. \tag{4}$$

From the approximate relationship between IWV and the observed ZWD derived by [39]:

$$\mathrm{ZWD} = 10^{-6} \mathrm{R_v} \int_0^\infty \rho_v(z) \left[k_2' + \frac{k_3}{T(z)}\right] dz, \tag{5}$$

and following the definition of T_m of [37]:

$$T_m = \frac{\int_0^\infty \rho_v(z) dz}{\int_0^\infty \frac{\rho_v(z)}{T(z)} dz}, \tag{6}$$

and combining the equation of state of water vapor, and the equations (2)–(6), as in [1], and following the formalism proposed by [37] and from [38], and rearranging them:

$$\mathrm{IWV} = \kappa(T_m) \times \mathrm{ZWD}, \tag{7}$$

where

$$\kappa(T_m) = 10^{-6} R_v \left[k_2' + \frac{k_3}{T_m}\right]. \tag{8}$$

We also used the following equation to calculate IWV:

$$\mathrm{gm}(\varphi, \mathrm{H}) = 9.784[1 - 0.00266 \cos(2\varphi) - 0.00000028\ \mathrm{H}], \tag{9}$$

where φ and H are the latitude and the height of the surface above the ellipsoid, respectively. To calculate T_s and P_s at the level of the receiver, to correct the differences of the height between the meteorological sensors and the GNSS receiver, we used the auxiliary equations as recommended by [40]:

$$T_2 = T_1 + \alpha(z_2 - z_1) \tag{10}$$

and

$$P_2 = P_1 \left(\frac{T_2}{T_1}\right)^{-g_0/\alpha R_d}, \tag{11}$$

where α is the temperature lapse rate (-6.5 K km^{-1}), and T_1 and P_1 are the observed temperature and pressure at the initial height z_1, R_d=287.027 J K^{-1} kg^{-1} (including CO_2) and g_0=9.80665 m s^{-2}.

The other constants used to calculate IWV are: M_v = 18.0152 (g mol^{-1}), M_d = 28.9644 (g mol^{-1}), k_1 = 77.600 (K hPa^{-1}), k_2 = 70.4 (K hPa^{-1}), k_3 = 3.739×10^3 (K^2 hPa^{-1}), $k_2' = k_2 - k_1[M_v/M_d]$ (K hPa^{-1}), R_v = 461.522 (J K^{-1} kg^{-1}).

Preprints (www.preprints.org) | NOT PEER-REVIEWED | Posted: 11 October 2019 doi:10.20944/preprints201910.0123.v1

Peer-reviewed version available at Remote Sens. 2019, 11, 2652; doi:10.3390/rs11222652

The actual value for T_m is expected to change due to the dependence on surface temperature, and tropospheric temperature profile, and on the vertical distribution of the atmosphere [1]. However, we adopted the common approximation of $T_m = 70.2 + 0.72*T_s$ [1] for the absent of frequent radiosonde, and for the purpose of this research.

We used GPS observation (RINEX files) data to perform zero-differenced Precise Point Positioning (PPP) technique with Bernese GNSS Software version 5.2 [41] to estimate tropospheric parameters. The collected data were processed in 24-hour sessions starting at 0000 UTC each day with data sampling of 30 second. We employed and adjusted the extended version of the PPP strategy (PPP_DEMO.PCF) to obtain high-rate tropospheric parameters with 15 minutes sampling. We applied the dry and wet terms of the Vienna Mapping Function 1 (VMF1)[2] [42] together with the European Centre for Medium-Range Weather Forecasts (ECMWF)–based zenith path delays corrections. Horizontal tropospheric gradients were estimated every 24 hours using Chen-Herring gradient model [43]. We used the value of 3° for the low elevation cut-off angle in all processing data.

All ZTD estimates passed by mandatory quality-control to avoid erroneous observations. Following the approach proposed by [44] and developed by [45], the screening procedure, aimed at detecting and removing the ZTD estimates that were physically out of range and/or less accurate value, was applied. ZTD data were screened concerning (i) the range check (reject ZTD values outside of 1 and 3 m), (ii) the outlier check (reject ZTD values outside of median[ZTD] ± 0.5 m), (iii) σ_{ZTD} range check (reject σ_{ZTD} values outside of 0.1 and 6 mm), and σ_{ZTD} outlier check (reject σ_{ZTD} values > 2 × median[σ_{ZTD}]).

Additional IWV products of were used to complement the comparisons against GNSS IWV estimates.

2.3. MODIS- and Radiosonde-Derived IWV

The MODIS MOD07 and MYD07 are products from the satellites TERRA (launched in 1999) and AQUA (launched in 2002), respectively. These products provide, among other resources, atmospheric profiles of water vapor IR-based estimates[3] in a 5 × 5 km resolution in clear scenes (for details and downloading the dataset see [46-50]). TERRA (AQUA) satellite overpasses the region of this research twice per day in the intervals of 0900–1045 and 2200–2315 (0030–0230 and 1245–1430) local time (LT).

MODIS IWV estimates were used for areal averages and for the comparisons with GNSS IWV estimates in the nearest grid of the respective GNSS receiver.

Radiosonde-derived IWV[4] was also used for comparisons with GNSS IWV although the GNSS receivers were not collocated in the neighborhood of the radiosonde launching site. The Vaisala RS92-SGP [51] radiosondes are launched twice-daily before the standard time of 0900 and 2100 LT.

Both MODIS and radiosonde IWV estimates were used for comparisons with GNSS-derived IWV in the period from January 2015–August 2018.

3. Results and Discussion

3.1. Analysis of GNSS-derived ZTD

Variations in the elevation in a region imply differences in the distribution of GNSS-derived ZTD. We used ZTD time series from the iGMAS station and compare them with those from the RBMC stations ONRJ and RIOD. The latter stations are located 4 and 12 km away from RDJN; and they differ in -8 cm and 27 m, respectively, with respect to the elevation of RDJN (see Table 1). Figure 2 shows the time series of ZTD (top panel) and statistics ZTD differences (lower panel) from RDJN in the

[2] Available for download at http://vmf.geo.tuwien.ac.at/.

[3] The Total Column Precipitable Water Vapor—IR Retrieval—is identified in the MODIS products in the subset "Atmospheric Profiles".

[4] The radiosonde derived IWV estimates were obtained directly from the Wyoming University website: http://weather.uwyo.edu/upperair/sounding.html.

Peer-reviewed version available at *Remote Sens.* **2019**, *11*, 2652; doi:10.3390/rs11222652

period of January 2015–August 2018. The long-term time series (with 91 065 samples) showed the general pattern of seasonal variations, and high variability of the differences in the small scale with occasional spikes. The total ZTD averages were 2.528/2.528/2.542 m for RDJN/ONRJ/RIOD. The mean, STD, and RMS of ZTD differences between RDJN and ONRJ were -0.40 mm, 1.90 mm, and 1.94 mm, respectively; while the mean, STD, and RMS of the differences between RDJN and RIOD were -14.28 mm, 6.04 mm, and 15.51 mm, respectively. For every 3-hour period, the mean difference between ZTD$_{RDJN}$ and ZTD$_{ONRJ}$ had the lowest (highest) values of -0.24 (-0.60) mm from 0900–1200 (0000–0245) LT; while the mean differences between ZTD$_{RDJN}$ and ZTD$_{RIOD}$ had the lowest (highest) values of -13.27 (-15.27) mm from 0600–0845 (1500–1745) LT.

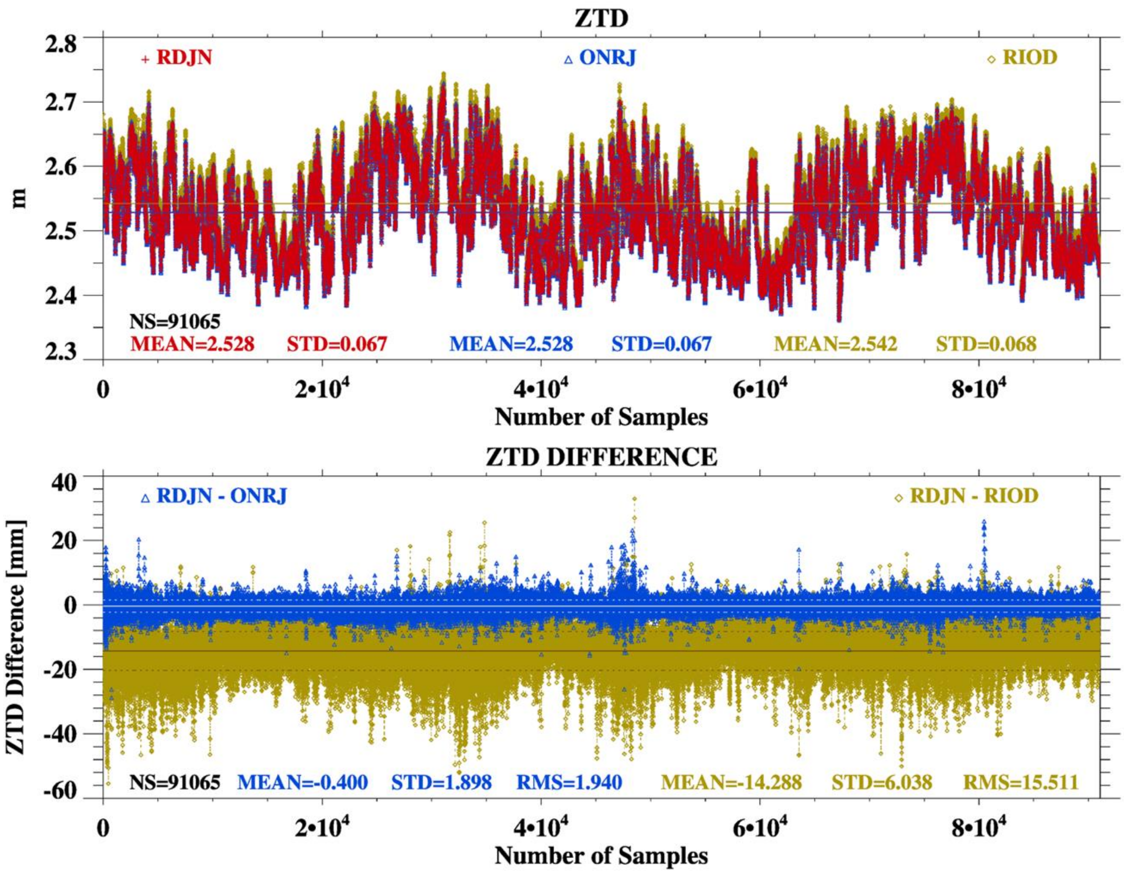

Figure 2. Time series, and number of samples (NS), mean, standard deviation (STD) of ZTD (upper panel) for the stations RDJN, ONRJ, and RIOD; and statistics (NS, mean, STD, and root mean square (RMS)) of ZTD differences (lower panel) from RDJN in the period of January 2015–August 2018.

The differences between ZTD$_{RDJN}$ and ZTD$_{ONRJ}$ could be primary related to instrumental errors, due to different receiver brand and model, hardware; the phase center variations; strategies used; and/or multipath effects (see e.g. [14,52-56]). On the other hand, RDJN and RIOD were not necessarily under the same atmospheric conditions as RDJN and ONRJ were. The differences between RDJN and RIOD must had first order components the differences in altitude and atmospheric conditions, as it is discussed in following sections.

3.2 Meteorological Conditions

We analyzed the meteorological conditions prevailing in six sites in the city of Rio de Janeiro, and in the stations named XE and CA located in the municipalities of *Xerém* and *Campos dos Goytacazes* (36 NNE and 233 km ENE from Rio de Janeiro), respectively. Figure 3 provides a general view of the mean (and standard deviation) of the 15-minute resolution diurnal cycle of *T* and relative humidity (*RH*) during the year 2015. (It is worth to report that the meteorological variables statistics were calculated for the period of January 2015–August 2018 for all stations, except for the station RI that became inoperant by late 2015. The mean patterns found for the entire period (not shown) were close to those presented for the year 2015 only.) There was large variability of *T and RH* with a well-defined diurnal cycle in continental sites in contrast with a small amplitude of *T* and *RH* in the near-oceanic sites. Moreover, Figure 3 highlights the diurnal cycle of *T* and *RH* for the sites RI/RD against FC/XE due to their evident differences. The highest (lowest) mean values of *T* (*RH*) in the diurnal cycle were observed in the sites RI and RD (XE and FC), with expressive differences of the mean *T* (*RH*) as high as 5 °C (30%). Large values of *RH* were found in the afternoon hours at FC, located by the coast, and in the nocturnal hours at XE, located near the northern mountain ranges that favor high convergence and convective activity in the foothills. (See Figure 1 that shows higher records of rainfall in XE than those in the other two sites with recorded rainfall.)

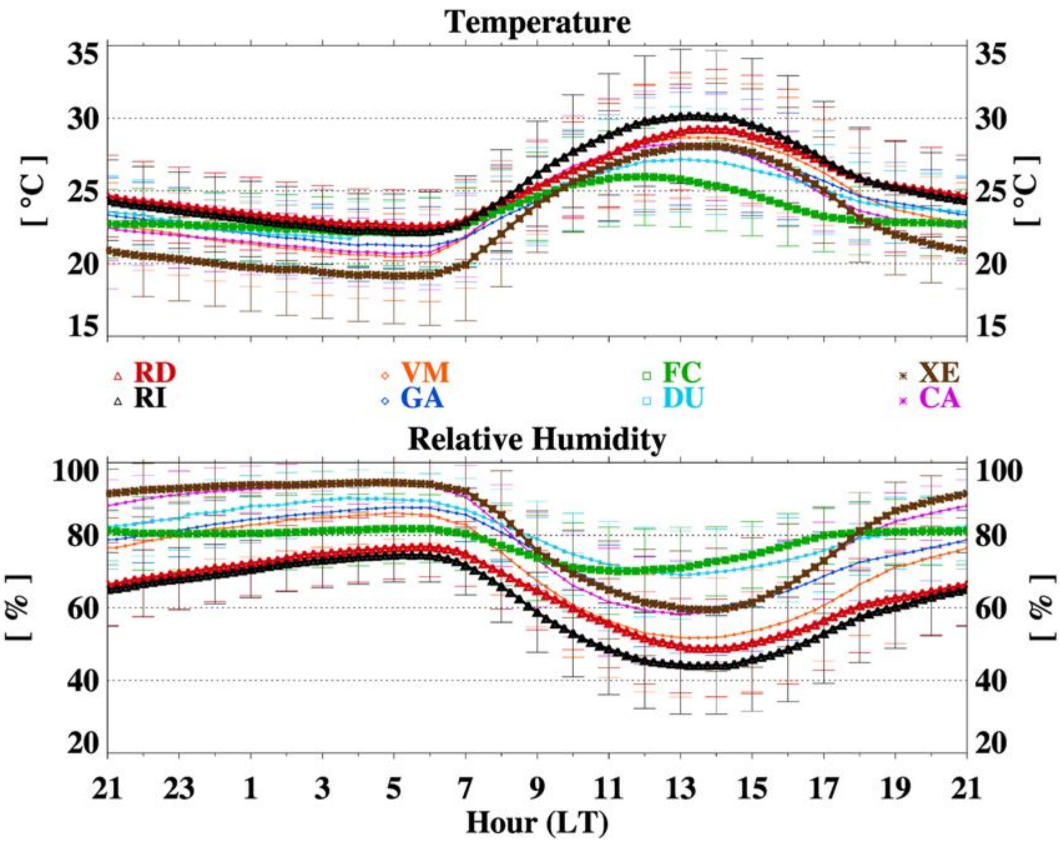

Figure 3. Fifteen-minute resolution diurnal cycle of the mean surface air temperature (*T*) and relative humidity (*RH*) and hourly standard deviation (STD) error bars from eight sites in the metropolitan area of Rio de Janeiro (MARJ) and *Campos dos Goytacazes* during 2015.

The spatial and temporal variabilities of *T* between the sites analyzed in this work corroborate with the observations of [23-25] that mapped urban, suburban, and rural heat islands in the MARJ. The authors of [23] indicated that the temperatures of the surface and the air near the surface in the heat islands were much higher than those in the surrounding (vegetated or near the cost) areas and were related with extreme rainfall events. Based on those maps and the results from this study, we suggested that *T* at RDJN/ONRJ, and RIOD were influenced by heat islands. Thus, the relation between the occurrence of heat islands and the meteorological variables such as *T*, winds, and precipitation, could lead to a heterogeneous distribution of T_m in the region.

T_m is commonly used to estimate IWV [1], which is highly correlated with the observed surface *T* and water vapor pressure (*e*) [57,58]. We compared the three-hour statistics of *T* and *e* from four different inputs (available from 2015–2018) with those from the site RI that is available only in the year 2015. With these comparisons we tested T_m, and hence IWV for RIOD, and applied the best approximation of meteorological variables for that site in the entire period of this research. Table 2 shows the statistics for two periods (0000–0245 LT and 1200–1445 LT) of the variables (vars) *T*, *e*, and

Preprints (www.preprints.org) | NOT PEER-REVIEWED | Posted: 11 October 2019 doi:10.20944/preprints201910.0123.v1

Peer-reviewed version available at *Remote Sens.* **2019**, *11*, 2652; doi:10.3390/rs11222652

T_m for RI and IWV in relation with other four sites. The comparisons of the matches were not linear, however they had significant different values of the variables within the sites, except the comparisons against those of the site RD. The meteorological conditions for the matches RI and RD were reasonably similar, with lower differences and higher statistical significance than those of RI and the other sites.

Table 2. Statistics (number of samples (NS), mean, STD, root mean square (RMS), and the correlation coefficient (R)) of the differences of the variables (vars): observed *T*, water vapor pressure (*e*), T_m, and integrated water vapor (IWV) from the meteorological and GNSS data for the three-hour periods of (a) 0000–0245 local time (LT) and (b) 1200–1445 LT for the year 2015.

(a) 0000–0245 LT with NS = 1648					
Stations:	**RI**	**RD**	**VM**	**FC**	**XE**
Var: *T*	22.700	23.072	21.086	21.936	19.483
DIFF.	**Diff. [°C]**	**Diff. [%]**	**STD [K]**	**RMS [K]**	**R**
RI-RD	-0.372	-1.639	0.541	0.656	0.973
RI-VM	1.613	7.108	1.425	2.152	0.856
RI-FC	0.764	3.367	1.502	1.685	0.777
RI-XE	3.217	14.173	2.415	4.022	0.657
Stations:	**RI**	**RD**	**VM**	**FC**	**XE**
Var: *e*	19.344	20.319	20.842	21.322	21.060
DIFF.	**Diff. [hPa]**	**Diff. [%]**	**STD [hPa]**	**RMS [hPa]**	**R**
RI-RD	-0.975	-5.043	1.008	1.403	0.954
RI-VM	-1.580	-8.166	1.929	2.493	--
RI-FC	-1.978	-10.225	1.210	2.318	0.914
RI-XE	-1.716	-8.871	2.037	2.663	0.829
Stations:	**RI**	**RD**	**VM**	**FC**	**XE**
Var: T_m	286.744	286.007	286.001	285.019	285.318
DIFF.	**Diff. [K]**	**Diff. [%]**	**STD [K]**	**RMS [K]**	**R**
RIOD[(RI)-(RD)]	0.737	0.257	0.818	1.101	0.963
RIOD[(RI)-(VM)]	0.744	0.259	0.606	0.959	0.978
RIOD[(RI)-(FC)]	1.726	0.602	1.655	2.391	0.810
RIOD[(RI)-(XE)]	1.426	0.497	0.777	1.624	0.961
Stations:	**RIOD(RI)**	**RIOD(RD)**	**RIOD(VM)**	**RIOD(FC)**	**RIOD(XE)**
Var: IWV	37.624	37.592	37.301	37.299	37.245
DIFF.	Diff. [mm]	Diff. [%]	STD [mm]	RMS [mm]	R
RIOD[(RI)-(RD)]	0.032	0.085	0.067	0.074	1.000
RIOD[(RI)-(VM)]	0.323	0.858	0.108	0.340	1.000
RIOD[(RI)-(FC)]	0.325	0.865	0.204	0.384	1.000
RIOD[(RI)-(XE)]	0.379	1.009	0.204	0.431	1.000

Peer-reviewed version available at Remote Sens. 2019, 11, 2652; doi:10.3390/rs11222652

(b) 1200–1445 LT with NS = 3133					
Stations:	**RI**	**RD**	**VM**	**FC**	**XE**
Var: *T*	29.543	28.590	28.159	25.103	27.519
DIFF.	**Diff. [°C]**	**Diff. [%]**	**STD [K]**	**RMS [K]**	**R**
RI-RD	0.953	3.225	1.218	1.546	0.965
RI-VM	1.384	4.685	1.007	1.712	0.976
RI-FC	4.440	15.027	2.872	5.288	0.763
RI-XE	2.024	6.849	1.253	2.380	0.958
Stations:	**RI**	**RD**	**VM**	**FC**	**XE**
Var: *e*	18.133	19.233	19.773	22.997	21.871
DIFF.	**Diff. [hPa]**	**Diff. [%]**	**STD [hPa]**	**RMS [hPa]**	**R**
RI-RD	-1.100	-6.067	1.265	1.676	0.926
RI-VM	-1.658	-9.144	3.431	3.810	--
RI-FC	-4.863	-26.820	2.336	5.395	0.728
RI-XE	-3.738	-20.612	1.800	4.148	0.884
Stations:	**RI**	**RD**	**VM**	**FC**	**XE**
Var: T_m	288.139	287.565	287.224	285.081	286.736
DIFF.	**Diff. [K]**	**Diff. [%]**	**STD [K]**	**RMS [K]**	**R**
RIOD[(RI)-(RD)]	0.574	0.199	0.877	1.048	0.965
RIOD[(RI)-(VM)]	0.914	0.317	0.725	1.167	0.976
RIOD[(RI)-(FC)]	3.058	1.061	2.068	3.692	0.763
RIOD[(RI)-(XE)]	1.403	0.487	0.902	1.668	0.958
Stations:	**RIOD(RI)**	**RIOD(RD)**	**RIOD(VM)**	**RIOD(FC)**	**RIOD(XE)**
Var: IWV	37.194	37.040	36.903	36.364	36.973
DIFF.	Diff. [mm]	Diff. [%]	STD [mm]	RMS [mm]	R
RIOD[(RI)-(RD)]	0.154	0.414	0.143	0.210	1.000
RIOD[(RI)-(VM)]	0.291	0.783	0.141	0.324	1.000
RIOD[(RI)-(FC)]	0.830	2.231	0.368	0.908	1.000
RIOD[(RI)-(XE)]	0.221	0.595	0.184	0.288	1.000

The mean ΔT (Δe), STD, and RMS were about -0.4 °C, 0.5 °C, and 0.7 °C (-1.98 hPa, 1.01 hPa, and 1.40 hPa), respectively for 0000-0245 LT; and the mean ΔT (Δe), STD, and RMS were about 1.0 °C, 1.2 °C, and 1.7 °C (-1.10 hPa, 1.26 hPa, and 1.77 hPa), respectively for 1200-1445 LT. The differences between the matches, in those two intervals, led to about 0.7/0.6 K and 0.03/0.15 mm respectively for ΔT_m and ΔIWV. The comparisons between the matches RI/XE and RI/FC showed high ΔT (Δe), up to 3.2/4.4 °C (-1.72/-4.89 hPa), led to relatively high values of 1.4/3.1 K and 0.38/0.83 mm for ΔT_m and Δ*IWV*, respectively.

From these comparisons, the best meteorological data used to estimate T_m, and hence IWV for the station RIOD in the period 2015–2018 were from the meteorological station RD. These comparisons showed low ΔT and Δe, less spread, and high accuracy between the matches RD and RI, and hence low ΔT_m and ΔIWV in the year 2015.

3.3 MODIS- versus GNSS-Derived IWV

Water vapor measurements from both MODIS satellites (TERRA and AQUA) provide an insightful complementary tool to analyze IWV jointly with GNSS-derived IWV. Figure 4 shows the temporal mean IWV of the daytime and nighttime overpasses of either MODIS TERRA or AQUA satellite in the MARJ. Two main patterns are observed in these panels: (i) a general underestimation of IWV in the nighttime averages; and (ii) a shifting of the highest values over the continent and over the ocean from daytime to nighttime. IWV distributions were marked by the largest values along the Atlantic coastline towards the upslopes of the mountain ranges during the daytime intervals (panels (b) and (c)). The nocturnal averages (panels (a) and (d)) showed the largest IWV values in the

 doi:10.20944/preprints201910.0123.v1

Peer-reviewed version available at *Remote Sens.* **2019**, *11*, 2652; doi:10.3390/rs11222652

atmosphere above the oceanic surface, indicating the presence of shifting breeze circulations in the diurnal cycle.

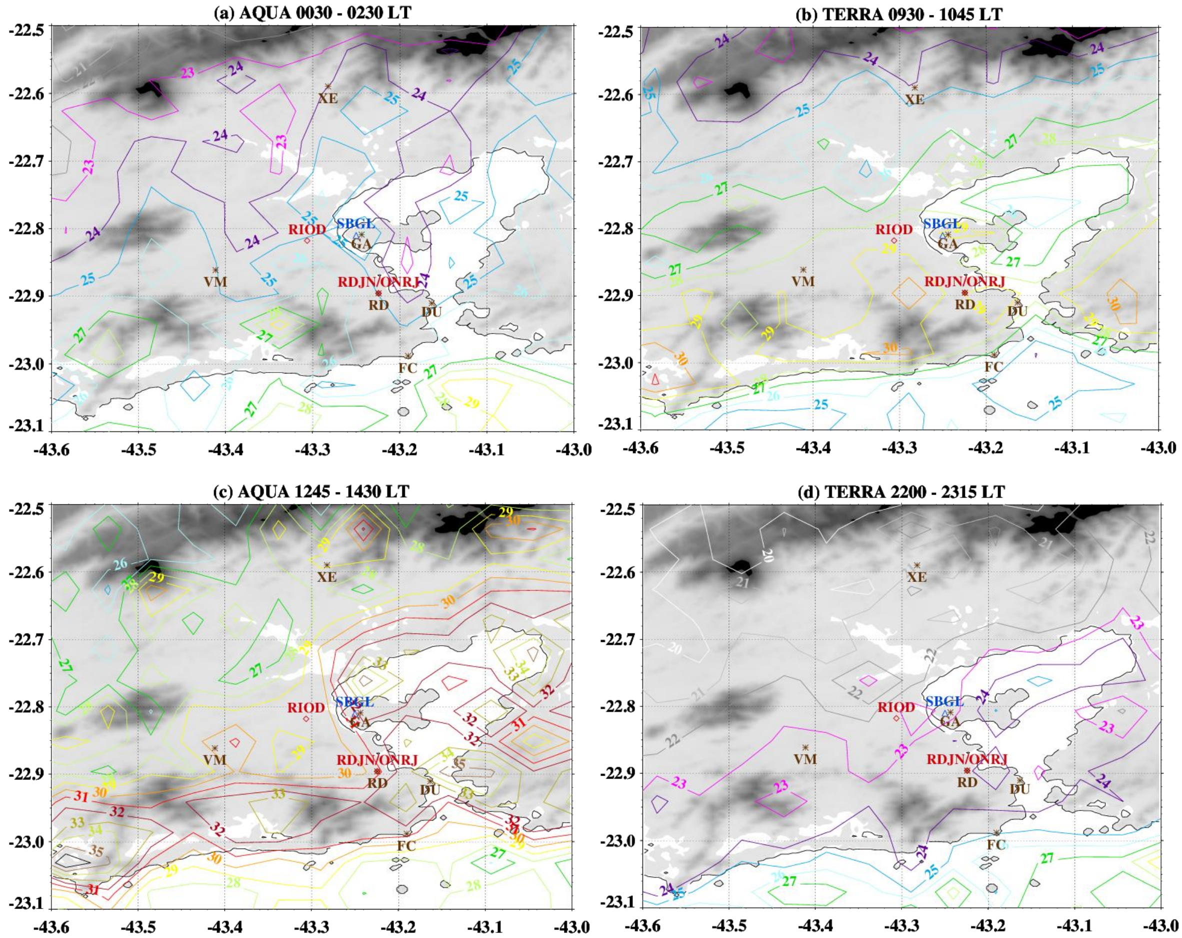

Figure 4. Mean MODIS IWV calculated from samplings of the twice-daily passages of the satellites AQUA (panels (a) and (c)) and TERRA (panels (b) and(d)) in a sector of Rio de Janeiro State.

High (low) IWV estimates during daytime (nighttime) by MODIS agree with the differences in the diurnal cycle of rainfall as calculated in three locations of the MARJ [12]; where minimum (maximum) rainfall occurred from late morning to the afternoon (late afternoon to evening) hours. The daytime convection seems to be influenced by land heating (such as the heat islands identified by [23-25]). Additionally, the convergence of the southerly and easterly sea breezes causes maxima rainfall from the coastline to the upslopes of the mountain ranges during the nocturnal hours (compare with [26-28]). These results explain why the number of samples of MODIS IWV estimates in daytime were higher than in nighttime, since MODIS measurements occur in absence of clouds, however the 5 × 5 km grid boxes could contain cloud pixels that absorb IR radiation, causing a dry bias in the total IWV sampled. The comparisons of MODIS- with GNSS-IWV provide additional information for the local estimates.

Table 3 presents the statistics of the IWV differences between MODIS and GNSS estimates. The nearest grid with MODIS IWV from the two daily passages of each satellite TERRA or AQUA were simultaneously collocated with the data from the GNSS stations RDJN/RIOD/RJCG. There was a general trend of MODIS-IWV to follow GNSS-IWV with relatively high correlation coefficient (above 0.84) for all matches. The differences between IWV_{MODIS} and IWV_{RDJN} in the daytime comparisons were from 0.8–1.1 mm (equivalent to percentage differences of about 2.6–4%); while the differences of IWV_{MODIS} against IWV_{RIOD} and IWV_{RJCG} were from -2–-0.7 (equivalent to percentage differences of about -6.5–-2.2%)[5]. Although the STD and RMS were relatively high (from 4.3–6.5 mm) for the diurnal estimates, the mean differences and correlation results were comparable with the acceptable ranges observed in previous comparisons of MODIS and GNSS IWV such as [59-62]. However, MODIS predominantly underestimated IWV against all GNSS estimates in the nocturnal passages, as observed in the areal averages. High percentages of the differences (of -37.4–-10.5% from MODIS) correspondent to mean differences from -8.6–-3 mm, STD from 4–5 mm (slightly lower than for daytime comparisons), and RMS from about 4.7–9.5 mm.

Table 3. Statistics (NS, mean, STD, RMS, and R) of estimates in the nearest point of MODIS-IWV and GNSS-IWV differences in the stations RDJN, RIOD, and RJCG. Grey (yellow) shaded rows highlight the comparisons of nocturnal (diurnal) passages of the satellites AQUA or TERRA.

Local Time	AQUA		RDJN	Local Time	TERRA	RDJN
0030-0230	25.085		28.016	0930-1045	28.942	27.816
1245-1430	30.179		29.408	2200-2315	23.617	28.316
MODIS	**NS**	**Diff. (mm)**	**Diff. [%]**	**STD (mm)**	**RMS (mm)**	**R**
AQUA[night]	223	-2.931	-10.462	4.999	5.785	0.841
TERRA[day]	217	1.125	4.046	5.273	5.379	0.887
AQUA[day]	242	0.771	2.622	5.578	5.620	0.891
TERRA[night]	145	-4.699	-16.596	4.406	6.431	0.889

Local Time	AQUA		RIOD	Local Time	TERRA	RIOD
0030-0230	26.242		31.143	0930-1045	29.564	30.239
1245-1430	30.707		31.461	2200-2315	23.456	30.768
MODIS	**NS**	**Diff. (mm)**	**Diff. [%]**	**STD (mm)**	**RMS (mm)**	**R**
AQUA[night]	234	-4.901	-15.736	4.683	6.772	0.883
TERRA[day]	278	-0.675	-2.232	4.729	4.769	0.920
AQUA[day]	324	-0.755	-2.399	6.499	6.533	0.873
TERRA[night]	204	-7.313	-23.767	4.371	8.514	0.887

Local Time	AQUA		RJCG	Local Time	TERRA	RJCG
0030-0230	25.687		31.627	0930-1045	29.575	31.491
1245-1430	31.495		32.582	2200-2315	23.130	31.778
MODIS	**NS**	**Diff. (mm)**	**Diff. [%]**	**STD (mm)**	**RMS (mm)**	**R**
AQUA[night]	266	-5.940	-23.123	3.904	7.104	0.880
TERRA[day]	258	-1.916	-6.477	4.287	4.688	0.928
AQUA[day]	290	-1.087	-3.452	5.107	5.212	0.911
TERRA[night]	244	-8.649	-37.391	3.917	9.491	0.890

3.4 Radiosonde- versus GNSS-Derived IWV

The comparisons of GNSS-IWV with the twice-daily radiosonde-IWV (RADS 0900 LT and 2100 LT) are used to evaluate the performances of IWV estimates for RDJN, ONRJ, and RIOD. Despite the disadvantage of the non-instantaneous measurements of the radiosonde observations, since the soundings are launched about 30 minutes before the standard time (ST), and the soundings last from 1–2 hours [63], we firstly tested the mean differences between GNSS-IWV at the ST of the radiosonde launching [i] and 4 different scenarios: [ii] 30 minutes before ST, [iii] 15 minutes before ST, [iv] 15 minutes after ST, and [v] 30 minutes after ST (Table 4).

[5] The comparisons of MODIS against GNSS IWV in intervals of low, intermediate, and high IWV values (not shown) presented high spam of the differences, more spread, and low correlation between the matches, probably related with small number of samples considered.

Preprints (www.preprints.org) | NOT PEER-REVIEWED | Posted: 11 October 2019 doi:10.20944/preprints201910.0123.v1

Peer-reviewed version available at Remote Sens. 2019, 11, 2652; doi:10.3390/rs11222652

Table 4. NS, mean, STD, and RMS of the differences between GNSS IWV on the ST (scenario [i]) and the scenarios [ii] 30 minutes before ST, [iii] 15 minutes before ST, [iv] 15 minutes after ST, [v] 30 minutes after ST, and the mean (shaded rows) of the scenarios [i], [ii], and [iii] for the two-daily soundings of (a) 0900 LT and (b) 2100 LT in the period from January 2015–August 2018.

(a) 0900 LT	RDJN[i] = 34.745		ONRJ[i] = 34.778	RIOD[i] = 35.720	
NS = 834	Diff. [mm]	Diff. [%]	STD [mm]	RMS [mm]	R
RDJN[i]-RDJN[ii]	-0.004	-0.012	0.654	0.653	0.999
ONRJ[i]-ONRJ[ii]	-0.025	-0.073	0.641	0.641	0.999
RIOD[i]-RIOD[ii]	0.003	0.010	0.798	0.798	0.998
RDJN[i]-RDJN[iii]	0.010	0.030	0.394	0.394	0.999
ONRJ[i]-ONRJ[iii]	-0.008	-0.023	0.398	0.398	0.999
RIOD[i]-RIOD[iii]	-0.008	-0.021	0.502	0.502	0.999
RDJN[i]-RDJN[iv]	-0.005	-0.014	0.366	0.366	--
ONRJ[i]-ONRJ[iv]	-0.004	-0.010	0.386	0.385	--
RIOD[i]-RIOD[iv]	0.004	0.012	0.468	0.468	--
RDJN[i]-RDJN[v]	-0.031	-0.088	0.629	0.629	--
ONRJ[i]-ONRJ[v]	-0.027	-0.078	0.662	0.662	--
RIOD[i]-RIOD[v]	-0.028	-0.078	0.784	0.784	--
RDJN[i]-RDJN[vi]	0.002	0.006	0.337	0.337	1.000
ONRJ[i]-ONRJ[vi]	-0.011	-0.032	0.332	0.332	1.000
RIOD[i]-RIOD[vi]	-0.001	-0.004	0.414	0.414	0.999

(b) 2100 LT	RDJN[i] = 36.480		ONRJ[i] = 36.530	RIOD[i] = 37.579	
NS = 823	Diff. [mm]	Diff. [%]	STD [mm]	RMS [mm]	R
RDJN[i]-RDJN[ii]	-0.030	-0.082	0.702	0.702	0.998
ONRJ[i]-ONRJ[ii]	-0.023	-0.062	0.706	0.706	0.998
RIOD[i]-RIOD[ii]	-0.109	-0.291	0.808	0.815	0.998
RDJN[i]-RDJN[iii]	-0.011	-0.029	0.337	0.337	1.000
ONRJ[i]-ONRJ[iii]	-0.013	-0.036	0.338	0.338	1.000
RIOD[i]-RIOD[iii]	-0.036	-0.096	0.400	0.401	0.999
RDJN[i]-RDJN[iv]	0.025	0.068	1.140	1.140	--
ONRJ[i]-ONRJ[iv]	0.007	0.018	1.146	1.146	--
RIOD[i]-RIOD[iv]	-0.251	-0.668	1.607	1.626	--
RDJN[i]-RDJN[v]	0.032	0.088	1.218	1.218	--
ONRJ[i]-ONRJ[v]	0.005	0.014	1.202	1.201	--
RIOD[i]-RIOD[v]	-0.231	-0.614	1.607	1.622	--
RDJN[i]-RDJN[vi]	-0.013	-0.037	0.332	0.332	1.000
ONRJ[i]-ONRJ[vi]	-0.012	-0.033	0.334	0.334	1.000
RIOD[i]-RIOD[vi]	-0.049	-0.129	0.385	0.388	1.000

The mean differences between IWV at ST and those scenarios were quite small, with low percentage of the differences, and high correlation coefficient—nearly unbiased especially in the stations RDJN/ONRJ. The amplitudes of the differences between the scenarios for morning soundings were equal or lesser than 0.031 mm, and STD/RMS decayed from 0.641/0.784 [ii] to 0.394/0.502 [iii] and increased symmetrically from [iv] and [v] matches. The differences for the nocturnal soundings had amplitudes equal or lesser than 0.251 mm, with similar decaying compared with that in 0900 LT, but they increased up to 1.140/1.607 mm in the matches [iv] and [v].

According to a general view of these results, there were lower biases, lesser spread, and higher accuracy in the comparisons between IWV[ST] and IWV[ST-15minutes] than between IWV[ST] and others matches after ST. Therefore, the IWV differences between the scenario [i] and the scenarios [ii]

Preprints (www.preprints.org) | NOT PEER-REVIEWED | Posted: 11 October 2019 doi:10.20944/preprints201910.0123.v1

Peer-reviewed version available at *Remote Sens.* **2019**, *11*, 2652; doi:10.3390/rs11222652

and [iii] were lesser spread and had higher accuracy than against those of [iv] and [v]. We used an additional scenario [vi] as the mean IWV estimates of the scenarios [i], [ii], and [iii] (see the highlighted lines in Table 3) to compare with those from radiosonde at the ST.

Though the IWV differences between RADS minus $GNSS_{[ST]}$ and RADS minus $GNSS_{[mean(ST-30/ST-15/ST)]}$ were from -0.049–0.002 mm, but STD and RMS were from 0.3–0.4 mm. Furthermore, considering that approximately 90% of water vapor distribution is located in the lower troposphere [63,64], we had chosen the mean as an ideal values of GNSS-IWV. The mean from the time of launching to the time radiosondes reach the level of 500 hPa (correspondent to the first 5 km above mean sea level), approximately on the ST, could be used as a reasonable estimate to be used for comparison with non-instantaneous radiosonde-IWV. For the above, we adopted the scenario [vi] for the GNSS-IWV to compare them with radiosonde-IWV.

Figure 5 shows the time series and statistics of IWV differences between RADS (0900 and 2100 LT) and RDJN/ONRJ/RIOD (mean of the estimates at 0830, 0845, and 0900 LT and the mean of the estimates at 2030, 2045, and 2100 LT). There was a contrasting behavior between the two daily soundings, where radiosonde IWV estimates were higher than those of all three GNSS estimates, except against RIOD at 0900 LT. The mean differences between IWV_{RADS} and IWV_{RDJN}/IWV_{ONRJ}/ IWV_{RIOD} at 0900 LT were 0.81/0.76/-0.17 mm, with STD 1.25/1.26/1.27 mm, and RMS 1.49/1.47/1.28 mm. At nighttime, the mean IWV_{RADS} minus IWV_{RDJN}/IWV_{ONRJ}/IWV_{RIOD} were 2.30/2.25/ 1.17 mm, with STD of 1.45/1.47/1.39 mm, and RMS of 2.72/2.69/1.81 mm.

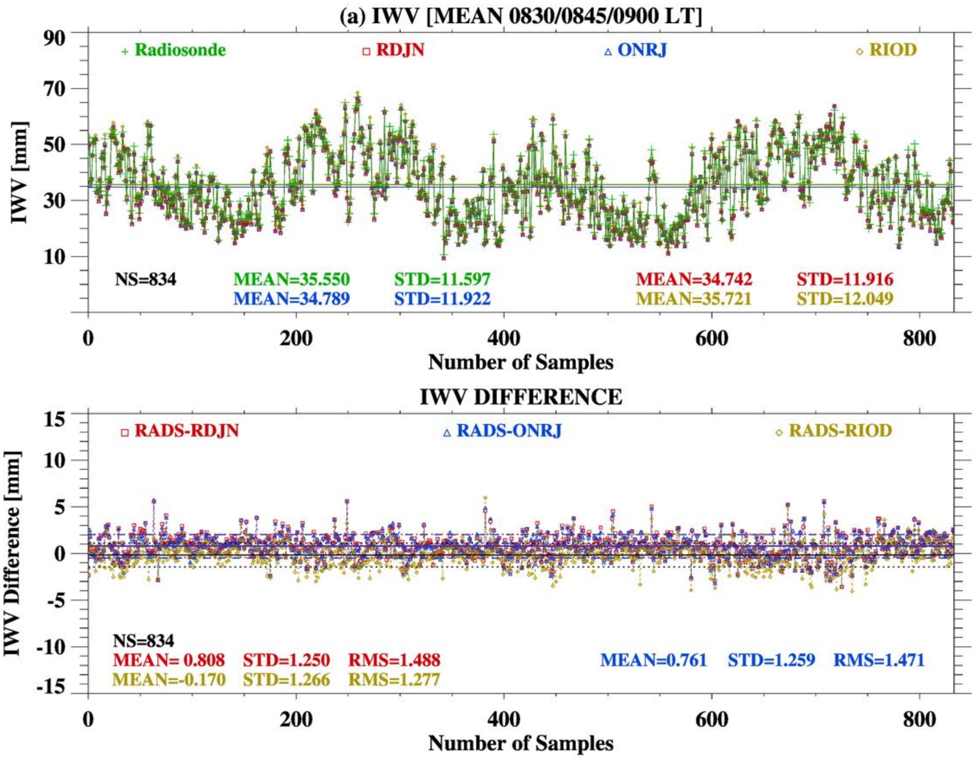

Preprints (www.preprints.org) | NOT PEER-REVIEWED | Posted: 11 October 2019 doi:10.20944/preprints201910.0123.v1

Peer-reviewed version available at Remote Sens. 2019, 11, 2652; doi:10.3390/rs11222652

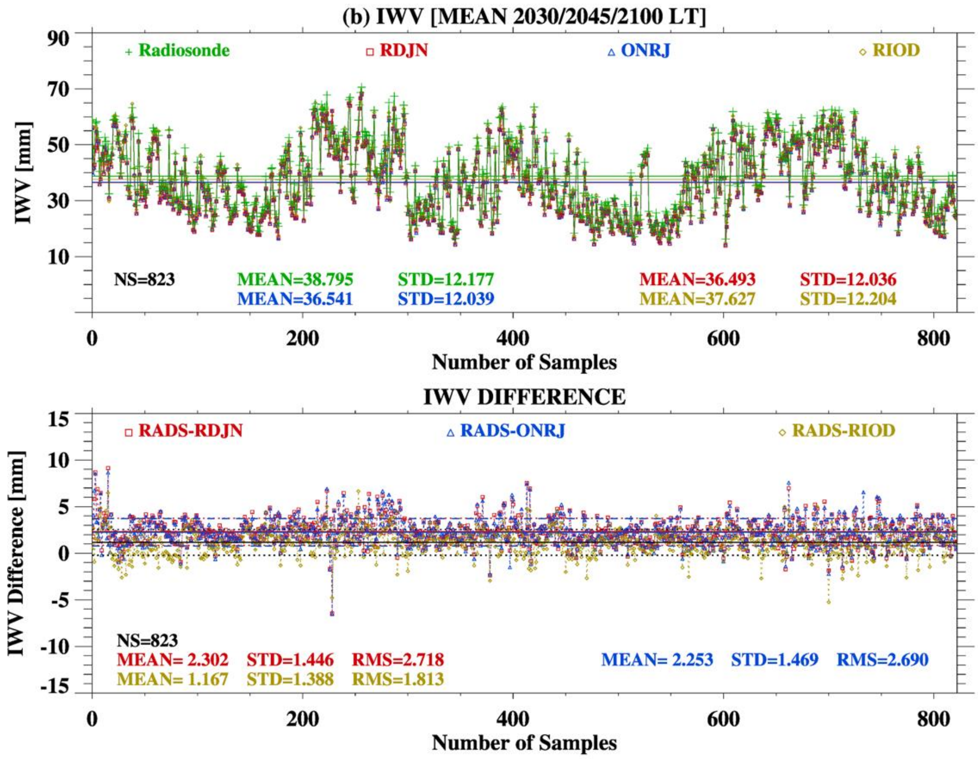

Figure 5. Time series and statistics (NS, mean, STD, and RMS) of Radiosonde- and GNSS-IWV and the differences from Radiosonde for (a) 0900 LT and (b) 2100 LT.

The statistics applied for three intervals of soundings of (a) low moisture ($IWV_{RADS} \leq 30$ mm), (b) intermediate moisture (30 mm < IWV_{RADS} < 50 mm), and (c) high moisture ($IWV_{RADS} \geq 50$ mm) are shown in Table 5. The comparisons between RADS and RDJN/ONRJ/RIOD were similar to those for all IWV estimates described above: radiosonde IWV was consistently 2.0/2.3/2.6 mm higher than those of $GNSS_{RDJN}$ (and $GNSS_{ONRJ}$), and 1.2/1.1/1.2 mm higher than those of $GNSS_{RIOD}$ in the intervals (a)/(b)/(c) at nighttime. As for the daytime soundings, IWV_{RADS} was about 1.0/1.6/2.2 (calculated by $Diff._{2100}$ minus $Diff._{0900}$) mm (or 4.0/4.0/3.9%) lower than it was expected in the interval (a)/(b)/(c) if not considered dry bias.

Table 5. Statistics (NS, mean, STD, RMS, and R) of radiosonde estimates for IWV intervals of (a) low moisture ($IWV_{RADS} \leq 30$ mm), (b) intermediate moisture (30 mm < IWV_{RADS} < 50 mm), and (c) high moisture ($IWV_{RADS} \geq 50$ mm) for the two-daily soundings in the period from January 2015–August 2018.

(a) Low moisture: RADS IWV ≤ 30 mm					
ST	**RADS**	**RDJN**		**ONRJ**	**RIOD**
0900 LT	23.345	22.274		22.298	23.072
NS = 300	Diff. [mm]	Diff. [%]	STD [mm]	RMS [mm]	R
RADS-RDJN	1.071	4.586	0.961	1.438	0.976
RADS-ONRJ	1.047	4.483	0.946	1.410	0.976
RADS-RIOD	0.273	1.169	1.001	1.036	0.975
ST	**RADS**	**RDJN**		**ONRJ**	**RIOD**
2100 LT	24.657	22.618		22.665	23.452
NS = 238	Diff. [mm]	Diff. [%]	STD [mm]	RMS [mm]	R
RADS-RDJN	2.040	8.273	0.994	2.268	0.959
RADS-ONRJ	1.993	8.082	1.013	2.235	0.957
RADS-RIOD	1.205	4.889	1.067	1.609	0.954

(b) Intermediate moisture: 30 mm < RADS IWV < 50 mm

Preprints (www.preprints.org) | NOT PEER-REVIEWED | Posted: 11 October 2019 doi:10.20944/preprints201910.0123.v1

Peer-reviewed version available at *Remote Sens.* **2019**, *11*, 2652; doi:10.3390/rs11222652

ST	**RADS**	**RDJN**	**ONRJ**	**RIOD**	
0900 LT	38.980	38.229	38.292	39.306	
NS = 415	Diff. [mm]	Diff. [%]	STD [mm]	RMS [mm]	R
RADS-RDJN	0.751	1.925	1.328	1.524	0.976
RADS-ONRJ	0.688	1.764	1.334	1.499	0.975
RADS-RIOD	-0.326	-0.838	1.286	1.325	0.977
ST	**RADS**	**RDJN**	**ONRJ**	**RIOD**	
2100 LT	39.464	37.147	37.184	38.356	
NS = 409	Diff. [mm]	Diff. [%]	STD [mm]	RMS [mm]	R
RADS-RDJN	2.317	5.872	1.429	2.721	0.970
RADS-ONRJ	2.280	5.777	1.475	2.714	0.968
RADS-RIOD	1.108	2.809	1.392	1.778	0.972
(c) High moisture: RADS IWV ≥ 50 mm					
ST	**RADS**	**RDJN**	**ONRJ**	**RIOD**	
0900 LT	54.364	54.017	54.063	55.111	
NS = 119	Diff. [mm]	Diff. [%]	STD [mm]	RMS [mm]	R
RADS-RDJN	0.347	0.638	1.454	1.489	0.927
RADS-ONRJ	0.301	0.553	1.499	1.522	0.924
RADS-RIOD	-0.747	-1.375	1.435	1.612	0.934
ST	**RADS**	**RDJN**	**ONRJ**	**RIOD**	
2100 LT	56.361	53.739	53.814	55.107	
NS = 176	Diff. [mm]	Diff. [%]	STD [mm]	RMS [mm]	R
RADS-RDJN	2.621	4.651	1.879	3.222	0.913
RADS-ONRJ	2.547	4.518	1.873	3.158	0.913
RADS-RIOD	1.254	2.225	1.726	2.129	0.925

As consequence of the inhomogeneity of altitude and meteorological conditions of the collocated stations used in this work, we observed that the atmosphere above RADS (located in an island) were about 2.3 mm wetter than above RDJN/ONRJ and 1.2 mm wetter than above RIOD at 2100 LT. The IWV differences between RDJN/ONRJ and RIOD remained consistently around 1.1 mm in the daytime (see next section for all 3-hour intervals), while IWV_{RADS} estimates would be 1.349 mm (or 3.656%) lower than it was expected in the absence of bias.

Despite the distances from RADS and RDJN/ONRJ and RIOD of 10 and 6 km, respectively, which contribute to meteorological differences in water vapor spatial distribution measured by GNSS receivers, the STD of the differences were below 3 mm as discussed by [19].

From our results, we infer that the lower differences at 0900 LT are due to a dry bias (for all intervals of the IWV estimates) in radiosonde during daylight time as observed comparable underestimation order of magnitude by [65,66] (see additionally [14,67-72]).

3.5 Space and Temporal Distributions of GNSS IWV in Rio de Janeiro

The estimates of GNSS-derived IWV for the data available in the city of Rio de Janeiro from January 2015–August 2018 are presented in this section. Table 6 shows IWV statistics for each three-hour period and for the entire dataset. High correlations between IWV_{RDJN} versus IWV_{ONRJ} and IWV_{RDJN} versus IWV_{RIOD} were observed, so that the periods of maxima IWV in all three locations occurred from the afternoon to nocturnal hours, and minima occurred from dawn to noon hours, with amplitude of the diurnal cycle of 1.872, 1.875, and 2.095 mm for RDJN, ONRJ, and RIOD, respectively. The mean diurnal cycle of IWV was consonant with that of rainfall as investigated by [12]. Slightly low correlation coefficient (0.996) between RDJN and RIOD was observed in the period of the day of increasing rate of IWV from noon–2100 LT, in comparison with the period from nocturnal–morning hours.

Table 6. Statistics (NS, Mean, STD, RMS, and R) of the IWV differences between RDJN and ONRJ and RIOD for every three-hour and the whole period from January 2015–August 2018.

0000–0245 LT	**RDJN = 36.137**		**ONRJ = 36.238**		**RIOD = 37.267**
NS = 11521	**Diff. [mm]**	**Diff. [%]**	**STD [mm]**	**RMS [mm]**	**R**
RDJN-ONRJ	-0.101	-0.278	0.310	0.326	1.000
RDJN-RIOD	-1.130	-3.126	0.915	1.454	0.997
0300–0545 LT	**RDJN = 35.441**		**ONRJ = 35.531**		**RIOD = 36.520**
NS = 11428	**Diff. [mm]**	**Diff. [%]**	**STD [mm]**	**RMS [mm]**	**R**
RDJN-ONRJ	-0.090	-0.253	0.267	0.282	1.000
RDJN-RIOD	-1.079	-3.043	0.838	1.366	0.998
0600–0845 LT	**RDJN = 34.995**		**ONRJ = 35.074**		**RIOD = 35.997**
NS = 11493	**Diff. [mm]**	**Diff. [%]**	**STD [mm]**	**RMS [mm]**	**R**
RDJN-ONRJ	-0.079	-0.226	0.278	0.289	1.000
RDJN-RIOD	-1.003	-2.865	0.845	1.311	0.998
0900–1145 LT	**RDJN = 34.906**		**ONRJ = 34.950**		**RIOD = 35.955**
NS = 10900	**Diff. [mm]**	**Diff. [%]**	**STD [mm]**	**RMS [mm]**	**R**
RDJN-ONRJ	-0.044	-0.125	0.291	0.294	1.000
RDJN-RIOD	-1.049	-3.004	0.957	1.420	0.997
1200–1445 LT	**RDJN = 35.295**		**ONRJ = 35.353**		**RIOD = 36.559**
NS=10825	**Diff. [mm]**	**Diff. [%]**	**STD [mm]**	**RMS [mm]**	**R**
RDJN-ONRJ	-0.057	-0.162	0.322	0.327	1.000
RDJN-RIOD	-1.264	-3.580	1.127	1.693	0.996
1500–1745 LT	**RDJN = 36.172**		**ONRJ = 36.219**		**RIOD = 37.533**
NS = 11164	**Diff. [mm]**	**Diff. [%]**	**STD [mm]**	**RMS [mm]**	**R**
RDJN-ONRJ	-0.046	-0.128	0.309	0.312	1.000
RDJN-RIOD	-1.360	-3.760	1.096	1.747	0.996
1800–2045 LT	**RDJN = 36.778**		**ONRJ = 36.825**		**RIOD = 38.050**
NS = 11251	**Diff. [mm]**	**Diff. [%]**	**STD [mm]**	**RMS [mm]**	**R**
RDJN-ONRJ	-0.048	-0.129	0.326	0.329	1.000
RDJN-RIOD	-1.273	-3.461	1.052	1.651	0.996
2100–2345 LT	**RDJN = 36.732**		**ONRJ = 36.820**		**RIOD = 38.017**
NS = 11555	**Diff. [mm]**	**Diff. [%]**	**STD [mm]**	**RMS [mm]**	**R**
RDJN-ONRJ	-0.088	-0.238	0.355	0.366	1.000
RDJN-RIOD	-1.285	-3.497	1.006	1.632	0.997
TOTAL MEAN	**RDJN**		**ONRJ**		**RIOD**
(mm)	**35.676**		**35.742**		**36.848**
NS = 85451	**Diff. [mm]**	**Diff. [%]**	**STD [mm]**	**RMS [mm]**	**R**
RDJN-ONRJ	-0.067	-0.187	0.302	0.309	1.000
RDJN-RIOD	-1.172	-3.285	0.982	1.529	0.997

The minimum (maximum) mean difference between IWV_{RDJN} and IWV_{ONRJ} were -0.101 (-0.044) mm for the time interval of 0000–0245 (0900–1145) LT, while the total mean, STD, and RMS were -0.067 mm, 0.302 mm, and 0.309 mm, respectively. More significant differences were found between IWV_{RDJN} and IWV_{RIOD} (comparing with those of the latter match), with the largest amplitude of the mean differences in the afternoon to evening hours (IWV_{RDJN} was 1.360 mm lower than IWV_{RIOD} in the period 1500–1745 LT), and the lowest amplitude of the mean differences in the nocturnal to morning hours (IWV_{RDJN} was 1.003 mm lower than IWV_{RIOD} from 0600–0845 LT) for the three-hour periods. The statistics of the differences between IWV_{RDJN} and IWV_{RIOD} for the entire dataset presented mean, STD, and RMS of -1.172 mm, 0.982 mm, and 1.529 mm, respectively. Similar to the above comparisons, the differences between IWV_{ONRJ} and IWV_{RIOD} were -1.1 mm. The latter comparison is

Preprints (www.preprints.org) | NOT PEER-REVIEWED | Posted: 11 October 2019 doi:10.20944/preprints201910.0123.v1

Peer-reviewed version available at Remote Sens. 2019, 11, 2652; doi:10.3390/rs11222652

similar to the results obtained by [19], who found -1.2 mm difference between IWV_{ONRJ} and IWV_{RIOD} in the period of about 7 years from 2007.

The comparisons of ZTD and IWV estimates between the RDJN, ONRJ, and RIOD highlighted the significant spatial differences between these sites. The consistent mean IWV difference between RDJN/ONRJ and RIOD indicates that those zones are influenced by different physiographical and meteorological conditions that request further investigation.

4. Conclusions

This study assessed the suitability of IWV estimates from the iGMAS GNSS ground-based receiver RDJN, and the comparisons with the estimates from the Brazilian network RBMC receivers ONRJ and RIOD in the metropolitan area of Rio de Janeiro, and the estimates for RJCG located in the city of *Campos dos Goytacazes* from January 2015–August 2018. We used additionally IWV estimates from the twice-daily radiosonde RADS located in the International Airport of *Galeão*, and the operational MODIS water vapor products MOD07 and MYD07 to evaluate the mean distribution of IWV in these regions.

Firstly, we analyzed the ZTD differences between RDJN and ONRJ, located on the roof of a building in the National Observatory, and the differences between RDJN and RIOD. ZTD statistics showed relatively small difference, STD, and RMS, respectively, -0.4 mm, 1.9 mm, and 1.9 mm, probably due to hardware differences and/or related with phase center variations, therefore they were neglected for the purpose of this research. Concerning the statistics for the matches RDJN and RIOD, there were higher values for the difference, STD, and RMS, respectively -14.3 mm, 6.0 mm, and 15.5 mm, as expected due to differences in elevation (where RDJN is located on a hill and RIOD in a valley) and meteorological conditions between these two sites 12 km apart from each other.

High variability of mean 15-minute diurnal cycle of T and RH were found between the sites. T (RH) mean differences as high as 5 °C (30%) between e.g. the sites RD/RI and FC/XE were suggested to be related with the occurrences of heat islands that have important effects in human weather comfortability and the formation of extreme weather events contributing to significant variability in the T_m, commonly used to estimate IWV. Mean differences in T and e, up to 4.4 °C and -4.89 hPa, respectively, between the matches RI and XE and the matches RI and FC, led to mean differences as high as 3.1 K for T_m and hence 0.83 mm for IWV. The spatial variability of surface temperature and meteorological conditions influenced by urban, suburban, and rural heat islands must be taken into account for best results of T_m and hence IWV. The usage of a complete meteorological data station collocated near every GNSS receiver is essential for improvements of IWV estimates, and it serves as an additional support for weather forecast by monitoring IWV locally.

The performance of MODIS MOD07 and MYD07 products, from respectively the satellites TERRA and AQUA, provided a reasonably good representation of the spatial mean distribution of IWV, especially during the daylight passages. It was observed IWV bands, in the diurnal averages, along the Atlantic coastline to the mountain upslopes, which were associated with high rainfall bands observed in previous studies.

The analyses of the comparisons between MODIS- and GNSS-derived IWV showed a general trend of MODIS to follow GNSS IWV with high correlation ($R \geq 0.84$) between the matches. IWV comparisons between the products from TERRA and AQUA and those from GNSS had mean differences of -2.4 to -0.7 mm (about -6 to 2% for MODIS against RJCG and RIOD) and 0.8 to 1.1 (about 2.6 to 4.0% for MODIS against RDJN) during daytime hours. However, some discrepancies were observed and were confirmed with relatively high random errors (STD in the order of 4 to 6 mm) and relatively low accuracy of the IWV estimates (RMS in the order of 5 to 9 mm). For most of the nocturnal samplings used in the comparisons, there were mean offset of -9 to -3 mm (about -37 to -10%) of MODIS with respect to GNSS.

Although MODIS, in the nocturnal hours, underestimates IWV comparing with GNSS-derived IWV and with relatively high RMS, the STD of these matches were slightly lower than those of the diurnal matches. After considering the advantages and weakness for IWV applications in this research, such as the systematic errors in the nocturnal hours, MODIS IWV products are reasonable

Preprints (www.preprints.org) | NOT PEER-REVIEWED | Posted: 11 October 2019 doi:10.20944/preprints201910.0123.v1

Peer-reviewed version available at Remote Sens. 2019, 11, 2652; doi:10.3390/rs11222652

good tools and can be used to investigate e.g. case studies of extreme rainfall and to validate IWV estimates for long time series either quantitatively in the diurnal hours and/or qualitatively in the nocturnal hours.

Concerning the non-instantaneous measurements of the radiosonde observations that could lead to errors in the comparisons with other estimates of water vapor, we found small biases (from -0.049 to 0.002 mm), but 0.3 mm of improvements when using the mean of GNSS estimates from the time of the launching to the standard time.

The comparisons of radiosonde- with GNSS-IWV revealed that the atmosphere above the portion of the island where RADS is located was 1.2 mm wetter than above RIOD (located in a valley) and 2.2 mm wetter than above RDJN/ONRJ at 2100 LT. These differences were explained as a consequence of the inhomogeneity of the altitude and the meteorological conditions between RADS, RIOD, and RDJN/ONRJ. On the other hand, the comparisons for the diurnal soundings had contrasting behavior where IWV_{RADS} minus IWV_{RIOD} was about -0.2 mm and IWV_{RADS} minus $IWV_{RDJN/ONRJ}$ was about 0.8 mm. Based on the differences between $IWV_{RDJN/ONRJ}$ and IWV_{RIOD}, which was about 1 mm, and that the differences between IWV_{RIOD} and IWV_{RADS} was also 1 mm, we conclude that there were dry bias caused by radiation in the radiosonde by 1.4 mm (or 3.7%) in the daytime soundings, similar to previous work. However, we cannot discard bias in GNSS IWV due to some other influences that were not computed in this work, especially due to the distances between the sites. The above lead us to recommend that comparisons of radiosonde IWV should consider separated daylight and nighttime analyses and the GNSS receiver should be collocated near the radiosonde launching site so the comparisons would be based in measurements of the same atmosphere.

The analyses of large number of samples of GNSS-based IWV from the iGMAS receiver and from the RBMC provided relevant insights on the water vapor distribution in the metropolitan area of Rio de Janeiro. The maxima GNSS IWV occur in the period from the afternoon to nocturnal hours, while the minima occur from dawn to noon hours, consonant with the periods of maxima and minima rainfall observed in the region. Small ZTD differences between RDJN and ONRJ were similar to the IWV differences; which were associated with instrumental errors that were neglected in the purpose of this research. However, the consistent mean differences between RDJN and RIOD of about -1 mm were indicated as result of the physiographic and meteorological differences, such as an easterly increment of moisture from the Guanabara Bay (near the RADS site) towards the valley at the North Zone of Rio de Janeiro where RIOD was located.

We learned from this research that the iGMAS RDJN dataset jointly with the RBMC GNSS-, MODIS-, and radiosonde-derived IWV products constituted powerful tool to investigate the distribution of water vapor in the region of Rio de Janeiro. The MARJ has unique physiographic and meteorological characteristics favoring the formation of extreme rainfall events that affect its population and demand additional studies. Composites of IWV with rainfall and case studies of extreme weather events related with the changes in IWV are subject of future research.

Funding: "The first author has been awarded by the CAS President's International Fellowship (PIFI) for Visiting Scientists at the Shanghai Astronomical Observatory (SHAO), Grant No. 2018VEB0007". "This study was supported by the key project of National Natural Science Fund (41730108) and the National Key R&D Program of China (2016YFB0501503-3)". "The co-author Katarzyna Stępniak has been supported by Polish National Science Centre, Grant No. UMO-2015/19/B/ST10/02758".

Acknowledgments: The authors acknowledge the International GNSS Monitoring and Assessment System (iGMAS) and IGS Multi-GNSS (MGEX) for providing the related data used in this study. INMET is specially acknowledged for providing part of the meteorological surface data. All personal from the *Observatório Nacional* in Rio de Janeiro related with the international cooperation with SHAO, specially Dr. Alexandre Andrei, for the installation, and maintenance of the iGMAS ground-based station RDJN installed at the ON. RBMC program is acknowledged for providing GNSS data online. The SHAO iGMAS and IGS/MGEX Analysis Center research group composed of staff members and graduate students are acknowledged for constant and indispensable support in Shanghai, especially Dr. Chen Qinming, Dr. Zhou Weili, and Li Wei. Acknowledgements to the *Universidade Federal do Pará* (UFPA) in Belém, Brazil, in which the first author is a government employee, and the colleagues and the staff at the Faculdade de Meteorologia (FAMET) and the *Instituto de Geociências* (IG), especially Dr. João Batista Miranda Ribeiro, Dr. Francisco de Souza Oliveira, Dr. Alexandre Casseb, Dr. Bergson Cavalcanti de Moraes, Dr. Glauber Guimarães Cirino da Silva, Dr. João de Athaydes Silva Júnior, Terezinha de Jesus da Silva Ferreira, and Marcelo Pamplona Carneiro, for their direct support.

References

1. Bevis, M.; Businger, S.; Herring, T.A.; Rocken, C.; Anthes, R.A.; Ware, R.H. GPS meteorology: Remote sensing of atmospheric water vapor using the global positioning system. *Journal of Geophysical Research* **1992**, *97*, 15787, doi:10.1029/92jd01517.
2. Bock, O.; Bosser, P.; Pacione, R.; Nuret, M.; Fourrié, N.; Parracho, A. A high-quality reprocessed ground-based GPS dataset for atmospheric process studies, radiosonde and model evaluation, and reanalysis of HyMeX Special Observing Period. *Quarterly Journal of the Royal Meteorological Society* **2016**, *142*, 56-71, doi:10.1002/qj.2701.
3. Deblonde, G.; Macpherson, S.; Mireault, Y.; Héroux, P. Evaluation of GPS Precipitable Water over Canada and the IGS Network. *Journal of Applied Meteorology* **2005**, *44*, 153-166, doi:10.1175/jam-2201.1.
4. Liou, Y.-A.; Teng, Y.-T.; Van Hove, T.; Liljegren, J.C. Comparison of Precipitable Water Observations in the Near Tropics by GPS, Microwave Radiometer, and Radiosondes. *Journal of Applied Meteorology* **2001**, *40*, 5-15, doi:10.1175/1520-0450(2001)040<0005:copwoi>2.0.co;2.
5. Mattioli, V.; Westwater, E.R.; Cimini, D.; Liljegren, J.C.; Lesht, B.M.; Gutman, S.I.; Schmidlin, F.J. Analysis of Radiosonde and Ground-Based Remotely Sensed PWV Data from the 2004 North Slope of Alaska Arctic Winter Radiometric Experiment. *Journal of Atmospheric and Oceanic Technology* **2007**, *24*, 415-431, doi:10.1175/jtech1982.1.
6. Rocken, C.; Van Hove, T.; Ware, R. Near real-time GPS sensing of atmospheric water vapor. *Geophysical Research Letters* **1997**, *24*, 3221-3224, doi:10.1029/97gl03312.
7. Song, S.; Zhu, W.; Ding, J.; Peng, J. 3D water-vapor tomography with Shanghai GPS network to improve forecasted moisture field. *Chinese Science Bulletin* **2006**, *51*, 607-614, doi:10.1007/s11434-006-0607-5.
8. Tregoning, P.; Boers, R.; O'Brien, D.; Hendy, M. Accuracy of absolute precipitable water vapor estimates from GPS observations. *Journal of Geophysical Research: Atmospheres* **1998**, *103*, 28701-28710, doi:10.1029/98jd02516.
9. Adams, D.K.; Fernandes, R.M.S.; Kursinski, E.R.; Maia, J.M.; Sapucci, L.F.; Machado, L.A.T.; Vitorello, I.; Monico, J.F.G.; Holub, K.L.; Gutman, S.I., et al. A dense GNSS meteorological network for observing deep convection in the Amazon. *Atmospheric Science Letters* **2011**, *12*, 207-212, doi:10.1002/asl.312.
10. Adams, D.K.; Fernandes, R.M.S.; Maia, J.M.F. GNSS Precipitable Water Vapor from an Amazonian Rain Forest Flux Tower. *Journal of Atmospheric and Oceanic Technology* **2011**, *28*, 1192-1198, doi:10.1175/jtech-d-11-00082.1.
11. Adams, D.K.; Gutman, S.I.; Holub, K.L.; Pereira, D.S. GNSS observations of deep convective time scales in the Amazon. *Geophysical Research Letters* **2013**, *40*, 2818-2823, doi:10.1002/grl.50573.
12. Mota, G.V.; Song, S. Extreme rainfall events observed by GNSS-derived ZTD and IWV in Rio de Janeiro. *Manuscript in preparation*, 2019.
13. Adams, D.K.; Fernandes, R.M.S.; Holub, K.L.; Gutman, S.I.; Barbosa, H.M.J.; Machado, L.A.T.; Calheiros, A.J.P.; Bennett, R.A.; Kursinski, E.R.; Sapucci, L.F., et al. The Amazon Dense GNSS Meteorological Network: A New Approach for Examining Water Vapor and Deep Convection

Interactions in the Tropics. *Bulletin of the American Meteorological Society* **2015**, *96*, 2151-2165, doi:10.1175/bams-d-13-00171.1.

14. Sapucci, L.F.; Machado, L.A.T.; Monico, J.F.G.; Plana-Fattori, A. Intercomparison of Integrated Water Vapor Estimates from Multisensors in the Amazonian Region. *Journal of Atmospheric and Oceanic Technology* **2007**, *24*, 1880-1894, doi:10.1175/jtech2090.1.
15. Smith, T.L.; Benjamin, S.G.; Gutman, S.I.; Sahm, S. Short-Range Forecast Impact from Assimilation of GPS-IPW Observations into the Rapid Update Cycle. *Monthly Weather Review* **2007**, *135*, 2914-2930, doi:10.1175/mwr3436.1.
16. Monico, J.F.G. GNSS: investigações e aplicações no posicionamento geodésico, em estudos relacionados com a atmosfera e na agricultura de precisão. *Projeto FAPESP na modalidade temático. Universidade Estadual Paulista. Presidente Prudente, SP* **2006**.
17. Sapucci, L.F.; Herdies, D.L.; Souza, R.V.A.D.; Mattos, J.G.Z.D.; Aravéquia, J.A. Os últimos avanços na previsibilidade dos campos de umidade no sistema global de assimilação de dados e previsão numérica de tempo do CPTEC/INPE. *Revista Brasileira de Meteorologia* **2010**, *25*, 295-310, doi:10.1590/s0102-77862010000300002.
18. Vitorello, I. Sistema Integrado de Posicionamento GNSS para Estudos Geodinâmicos. *Projeto aprovado e em andamento com recursos da PETROBRAS. Instituto Nacional de Pesquisas Espaciais - INPE/MCT. São José dos Campos* **2008**.
19. Bianchi, C.E.; Mendoza, L.P.O.; Fernández, L.I.; Natali, M.P.; Meza, A.M.; Moirano, J.F. Multi-year GNSS monitoring of atmospheric IWV over Central and South America for climate studies. *Annales Geophysicae* **2016**, *34*, 623-639, doi:10.5194/angeo-34-623-2016.
20. Gendt, G.; Dick, G.; Reigber, C.; Tomassini, M.; Liu, Y.; Ramatschi, M. Near Real Time GPS Water Vapor Monitoring for Numerical Weather Prediction in Germany. *Journal of the Meteorological Society of Japan. Ser. II* **2004**, *82*, 361-370, doi:10.2151/jmsj.2004.361.
21. Song, S.; Zhu, W.; Chen, Q.; Liou, Y. Establishment of a new tropospheric delay correction model over China area. *Science China Physics, Mechanics and Astronomy* **2011**, *54*, 2271-2283, doi:10.1007/s11433-011-4530-7.
22. Song, S.-L.; Zhu, W.-Y.; Ding, J.-C.; Liao, X.-H.; Cheng, Z.-Y.; Ye, Q.-X. Near Real-Time Sensing of PWV from SGCAN and the Application Test in Numerical Weather Forecast. *Chinese Journal of Geophysics* **2004**, *47*, 719-727, doi:10.1002/cjg2.3542.
23. Lucena, A.J.; Correa, E.B.; Rotunno Filho, O.C.; Peres, L.F.; França, J.R.A.; Justi da Silva, M.G.A. Ilhas de calor e eventos de precipitação na região metropolitana do Rio de Janeiro (RMRJ). *XIV World Water Congress and 10° SILUSBA* **2011**.
24. Lucena, A.J.; de Faria Peres, L.; Filho, O.C.R.; de Almeida Franca, J.R. Estimation of the urban heat island in the Metropolitan Area of Rio de Janeiro - Brazil. In Proceedings of 2015 Joint Urban Remote Sensing Event (JURSE), 2015/03.
25. Lucena, A.J.d.; Rotunno Filho, O.C.; França, J.R.d.A.; Peres, L.d.F.; Xavier, L.N.R. Urban climate and clues of heat island events in the metropolitan area of Rio de Janeiro. *Theoretical and Applied Climatology* **2012**, *111*, 497-511, doi:10.1007/s00704-012-0668-0.
26. Brandão, A.M.P.M. As alterações climáticas na área metropolitana do Rio de Janeiro: uma possível influência do crescimento urbano in Abreu, M. A in *Natureza e Sociedade no Rio de Janeiro* - Rio de Janeiro. Secetaria Municipal de Cultura, Turismo e Esportes **1992**, 143-200.

27. Dereczynski, C.P.; Oliveira, J.S.d.; Machado, C.O. Climatologia da precipitação no município do Rio de Janeiro. *Revista Brasileira de Meteorologia* **2009**, *24*, 24-38, doi:10.1590/s0102-77862009000100003.
28. Ferreira, F.P.M.; Cunha, S.B. Enchentes no Rio de Janeiro: efeitos da urbanização no Rio Grande (Arroio Fundo) - Jacarepaguá. *Anuário do Instituto dc Geociências* **1996**, *19*, 79-92.
29. IBGE (Instituto Brasileiro de Geografia e Estatística). Availabe online: https://www.ibge.gov.br/en/geosciences/downloads-geosciences.html (accessed on 9 September 2018).
30. IBGE (Instituto Brasileiro de Geografia e Estatística). RBMC - Rede Brasileira de Monitoramento Contínuo dos Sistemas GNSS. Availabe online: http://www.ibge.gov.br/home/geociencias/geodesia/rbmc/rbmc.shtm (accessed on 9 August 2019).
31. Fortes, L.P.S. Status of the Brazilian Network for Continuous Monitoring of GPS (RBMC). In *GPS Trends in Precise Terrestrial, Airborne, and Spaceborne Applications*, Springer Berlin Heidelberg: 1996; 10.1007/978-3-642-80133-4_13pp 85-88.
32. Fortes, L.P.S.; Luz, R.T.; Pereira, K.D.; Costa, S.M.A.; Blitzkow, D. The Brazilian Network for Continuous Monitoring of GPS (RBMC): Operation and Products. In *Advances in Positioning and Reference Frames*, Springer Berlin Heidelberg: 1998; 10.1007/978-3-662-03714-0_11pp 73-78.
33. INMET (Instituto Nacional de Meteorologia). Dados Meteorológicos: Estações Automáticas. Availabe online: http://www.inmet.gov.br/portal/index.php?r=estacoes/estacoesAutomaticas (accessed on 9 September 2018).
34. Danielson, J.J.; Gesch, D.B. Global multi-resolution terrain elevation data 2010 (GMTED2010). In *Open-File Report*, US Geological Survey: 2011; 10.3133/ofr20111073.
35. Lott, J.N.; Vose, R.S.; Del Greco, S.A.; Ross, T.R.; Worley, S.; J.L., C. The integrated surface database: Partnerships and progress. In Proceedings of 24th Conference on Interactive Information Processing Systems for Meteorology, Oceanography, and Hydrology (IIPS), New Orleans, LA.
36. Smith, A.; Lott, N.; Vose, R. The Integrated Surface Database: Recent Developments and Partnerships. *Bulletin of the American Meteorological Society* **2011**, *92*, 704-708, doi:10.1175/2011bams3015.1.
37. Davis, J.L.; Herring, T.A.; Shapiro, I.I.; Rogers, A.E.E.; Elgered, G. Geodesy by radio interferometry: Effects of atmospheric modeling errors on estimates of baseline length. *Radio Science* **1985**, *20*, 1593-1607, doi:10.1029/rs020i006p01593.
38. Saastamoinen, J. Atmospheric Correction for Troposphere and Stratosphere in Radio Ranging of Satellites. *The Use of Artificial Satellites for Geodesy, Geophysics Monograph Series* **1972**, *15*, 247-251, doi:10.1029/GM015p0247.
39. Askne, J.; Nordius, H. Estimation of tropospheric delay for microwaves from surface weather data. *Radio Science* **1987**, *22*, 379-386, doi:10.1029/rs022i003p00379.
40. Manual of the ICAO Standard Atmosphere (extended to 80 kilometres (262 500 feet). *ICAO International Civil Aviation Organization* **1993**.
41. Dach, R.; Lutz, S.; Walser, P.; Fridez, P. Bernese GNSS Software Version 5.2. User manual. *Astronomical Institute, University of Bern, Bern Open Publishing* **2015**.

Peer-reviewed version available at *Remote Sens.* **2019**, *11*, 2652; doi:10.3390/rs11222652

42. Boehm, J.; Werl, B.; Schuh, H. Troposphere mapping functions for GPS and very long baseline interferometry from European Centre for Medium-Range Weather Forecasts operational analysis data. *Journal of Geophysical Research: Solid Earth* **2006**, *111*, n/a-n/a, doi:10.1029/2005jb003629.
43. Chen, G.; Herring, T.A. Effects of atmospheric azimuthal asymmetry on the analysis of space geodetic data. *Journal of Geophysical Research: Solid Earth* **1997**, *102*, 20489-20502, doi:10.1029/97jb01739.
44. Bock, O.; Willis, P.; Wang, J.; Mears, C. A high-quality, homogenized, global, long-term (1993-2008) DORIS precipitable water data set for climate monitoring and model verification. *Journal of Geophysical Research: Atmospheres* **2014**, *119*, 7209-7230, doi:10.1002/2013jd021124.
45. Stepniak, K.; Bock, O.; Wielgosz, P. Reduction of ZTD outliers through improved GNSS data processing and screening strategies. *Atmospheric Measurement Techniques* **2018**, *11*, 1347-1361, doi:10.5194/amt-11-1347-2018.
46. Borbas, E., et al. MODIS Atmosphere L2 Atmosphere Profile Product. NASA MODIS Adaptive Processing System, Goddard Space Flight Center, USA, http://dx.doi.org/10.5067/MODIS/MOD07_L2.006. 2015.
47. Borbas, E., et al. MODIS Atmosphere L2 Atmosphere Profile Product. NASA MODIS Adaptive Processing System, Goddard Space Flight Center, USA, http://dx.doi.org/10.5067/MODIS/MYD07_L2.006. 2015.
48. Moeller, C.C.; Frey, R.A.; Borbas, E.; Menzel, W.P.; Wilson, T.; Wu, A.; Geng, X. Improvements to Terra MODIS L1B, L2, and L3 science products through using crosstalk corrected L1B radiances. In Proceedings of Earth Observing Systems XXII, 2017/09/05.
49. Seemann, S.W.; Borbas, E.E.; Knuteson, R.O.; Stephenson, G.R.; Huang, H.-L. Development of a Global Infrared Land Surface Emissivity Database for Application to Clear Sky Sounding Retrievals from Multispectral Satellite Radiance Measurements. *Journal of Applied Meteorology and Climatology* **2008**, *47*, 108-123, doi:10.1175/2007jamc1590.1.
50. Seemann, S.W.; Li, J.; Menzel, W.P.; Gumley, L.E. Operational Retrieval of Atmospheric Temperature, Moisture, and Ozone from MODIS Infrared Radiances. *Journal of Applied Meteorology* **2003**, *42*, 1072-1091, doi:10.1175/1520-0450(2003)042<1072:oroatm>2.0.co;2.
51. Oliveira, F.P.; Amorim, H.S.; Dereczynski, C.P. Investigando a atmosfera com dados obtidos por radiossondas. *Revista Brasileira de Ensino de Física* **2018**, *40*, no. 3, e3503, doi: http://dx.doi.org/10.1590/1806-9126-RBEF-2017-0352.
52. Buehler, S.A.; Östman, S.; Melsheimer, C.; Holl, G.; Eliasson, S.; John, V.O.; Blumenstock, T.; Hase, F.; Elgered, G.; Raffalski, U., et al. A multi-instrument comparison of integrated water vapour measurements at a high latitude site. *Atmospheric Chemistry and Physics* **2012**, *12*, 10925-10943, doi:10.5194/acp-12-10925-2012.
53. Jarlemark, P.; Emardson, R.; Johansson, J.; Elgered, G. Ground-Based GPS for Validation of Climate Models: The Impact of Satellite Antenna Phase Center Variations. *IEEE Transactions on Geoscience and Remote Sensing* **2010**, *48*, 3847-3854, doi:10.1109/tgrs.2010.2049114.
54. King, M.A.; Watson, C.S. Long GPS coordinate time series: Multipath and geometry effects. *Journal of Geophysical Research* **2010**, *115*, doi:10.1029/2009jb006543.

55. Ning, T.; Elgered, G.; Johansson, J.M. The impact of microwave absorber and radome geometries on GNSS measurements of station coordinates and atmospheric water vapour. *Advances in Space Research* **2011**, *47*, 186-196, doi:10.1016/j.asr.2010.06.023.
56. Ning, T.; Haas, R.; Elgered, G.; Willén, U. Multi-technique comparisons of 10 years of wet delay estimates on the west coast of Sweden. *Journal of Geodesy* **2011**, *86*, 565-575, doi:10.1007/s00190-011-0527-2.
57. Sapucci, L.F. Evaluation of Modeling Water-Vapor-Weighted Mean Tropospheric Temperature for GNSS-Integrated Water Vapor Estimates in Brazil. *Journal of Applied Meteorology and Climatology* **2014**, *53*, 715-730, doi:10.1175/jamc-d-13-048.1.
58. Yao, Y.; Zhang, B.; Xu, C.; Yan, F. Improved one/multi-parameter models that consider seasonal and geographic variations for estimating weighted mean temperature in ground-based GPS meteorology. *Journal of Geodesy* **2013**, *88*, 273-282, doi:10.1007/s00190-013-0684-6.
59. Alraddawi, D.; Sarkissian, A.; Keckhut, P.; Bock, O.; Noël, S.; Bekki, S.; Irbah, A.; Meftah, M.; Claud, C. Comparison of total water vapour content in the Arctic derived from GNSS, AIRS, MODIS and SCIAMACHY. *Atmospheric Measurement Techniques* **2018**, *11*, 2949-2965, doi:10.5194/amt-11-2949-2018.
60. Cimini, D.; Pierdicca, N.; Pichelli, E.; Ferretti, R.; Mattioli, V.; Bonafoni, S.; Montopoli, M.; Perissin, D. On the accuracy of integrated water vapor observations and the potential for mitigating electromagnetic path delay error in InSAR. *Atmospheric Measurement Techniques* **2012**, *5*, 1015-1030, doi:10.5194/amt-5-1015-2012.
61. Liu, Z.; Wong, M.S.; Nichol, J.; Chan, P.W. A multi-sensor study of water vapour from radiosonde, MODIS and AERONET: a case study of Hong Kong. *International Journal of Climatology* **2011**, *33*, 109-120, doi:10.1002/joc.3412.
62. Vaquero-Martínez, J.; Antón, M.; Ortiz de Galisteo, J.P.; Cachorro, V.E.; Costa, M.J.; Román, R.; Bennouna, Y.S. Validation of MODIS integrated water vapor product against reference GPS data at the Iberian Peninsula. *International Journal of Applied Earth Observation and Geoinformation* **2017**, *63*, 214-221, doi:10.1016/j.jag.2017.07.008.
63. Guerova, G.; Jones, J.; Douša, J.; Dick, G.; de Haan, S.; Pottiaux, E.; Bock, O.; Pacione, R.; Elgered, G.; Vedel, H., et al. Review of the state of the art and future prospects of the ground-based GNSS meteorology in Europe. *Atmospheric Measurement Techniques* **2016**, *9*, 5385-5406, doi:10.5194/amt-9-5385-2016.
64. Bevis, M.; Businger, S.; Chiswell, S.; Herring, T.A.; Anthes, R.A.; Rocken, C.; Ware, R.H. GPS Meteorology: Mapping Zenith Wet Delays onto Precipitable Water. *Journal of Applied Meteorology* **1994**, *33*, 379-386, doi:10.1175/1520-0450(1994)033<0379:gmmzwd>2.0.co;2.
65. Sapucci, L.F.; Machado, L.A.T.; da Silveira, R.B.; Fisch, G.; Monico, J.F.G. Analysis of Relative Humidity Sensors at the WMO Radiosonde Intercomparison Experiment in Brazil. *Journal of Atmospheric and Oceanic Technology* **2005**, *22*, 664-678, doi:10.1175/jtech1754.1.
66. Turner, D.D.; Lesht, B.M.; Clough, S.A.; Liljegren, J.C.; Revercomb, H.E.; Tobin, D.C. Dry Bias and Variability in Vaisala RS80-H Radiosondes: The ARM Experience. *Journal of Atmospheric and Oceanic Technology* **2003**, *20*, 117-132, doi:10.1175/1520-0426(2003)020<0117:dbaviv>2.0.co;2.
67. Bock, O.; Bouin, M.N.; Walpersdorf, A.; Lafore, J.P.; Janicot, S.; Guichard, F.; Agusti-Panareda, A. Comparison of ground-based GPS precipitable water vapour to independent observations

Peer-reviewed version available at *Remote Sens.* **2019**, *11*, 2652; doi:10.3390/rs11222652

and NWP model reanalyses over Africa. *Quarterly Journal of the Royal Meteorological Society* **2007**, *133*, 2011-2027, doi:10.1002/qj.185.

68. Dzambo, A.M.; Turner, D.D.; Mlawer, E.J. Evaluation of two Vaisala RS92 radiosonde solar radiative dry bias correction algorithms. *Atmospheric Measurement Techniques* **2016**, *9*, 1613-1626, doi:10.5194/amt-9-1613-2016.
69. Park, C.-G.; Roh, K.-M.; Cho, J.-H. Radiosonde Sensors Bias in Precipitable Water Vapor From Comparisons With Global Positioning System Measurements. *Journal of Astronomy and Space Sciences* **2012**, *29*, 295-303, doi:10.5140/jass.2012.29.3.295.
70. Van Baelen, J.; Aubagnac, J.-P.; Dabas, A. Comparison of Near–Real Time Estimates of Integrated Water Vapor Derived with GPS, Radiosondes, and Microwave Radiometer. *Journal of Atmospheric and Oceanic Technology* **2005**, *22*, 201-210, doi:10.1175/jtech-1697.1.
71. Wang, J.; Zhang, L. Systematic Errors in Global Radiosonde Precipitable Water Data from Comparisons with Ground-Based GPS Measurements. *Journal of Climate* **2008**, *21*, 2218-2238, doi:10.1175/2007jcli1944.1.
72. Wang, J.; Zhang, L.; Dai, A.; Immler, F.; Sommer, M.; Vömel, H. Radiation Dry Bias Correction of Vaisala RS92 Humidity Data and Its Impacts on Historical Radiosonde Data. *Journal of Atmospheric and Oceanic Technology* **2013**, *30*, 197-214, doi:10.1175/jtech-d-12-00113.1.